Circulation Research

ORIGINAL RESEARCH

Single-Cell Analysis of Blood-Brain Barrier Response to Pericyte Loss

Maarja A. Mäe, Liqun He, Sofia Nordling, Elisa Vazquez-Liebanas, Khayrun Nahar, Bongnam Jung, Xidan Li, Bryan C. Tan, Juat Chin Foo, Amaury Cazenave-Gassiot, Markus R. Wenk, Yvette Zarb, Barbara Lavina, Susan E. Quaggin, Marie Jeansson, Chengua Gu, David L. Silver, Michael Vanlandewijck, Eugene C. Butcher, Annika Keller, Christer Betsholtz

RATIONALE: Pericytes are capillary mural cells playing a role in stabilizing newly formed blood vessels during development and tissue repair. Loss of pericytes has been described in several brain disorders, and genetically induced pericyte deficiency in the brain leads to increased macromolecular leakage across the blood-brain barrier (BBB). However, the molecular details of the endothelial response to pericyte deficiency remain elusive.

OBJECTIVE: To map the transcriptional changes in brain endothelial cells resulting from lack of pericyte contact at single-cell level and to correlate them with regional heterogeneities in BBB function and vascular phenotype.

METHODS AND RESULTS: We reveal transcriptional, morphological, and functional consequences of pericyte absence for brain endothelial cells using a combination of methodologies, including single-cell RNA sequencing, tracer analyses, and immunofluorescent detection of protein expression in pericyte-deficient adult *Pdgfb*$^{ret/ret}$ mice. We find that endothelial cells without pericyte contact retain a general BBB-specific gene expression profile, however, they acquire a venous-shifted molecular pattern and become transformed regarding the expression of numerous growth factors and regulatory proteins. Adult *Pdgfb*$^{ret/ret}$ brains display ongoing angiogenic sprouting without concomitant cell proliferation providing unique insights into the endothelial tip cell transcriptome. We also reveal heterogeneous modes of pericyte-deficient BBB impairment, where hotspot leakage sites display arteriolar-shifted identity and pinpoint putative BBB regulators. By testing the causal involvement of some of these using reverse genetics, we uncover a reinforcing role for angiopoietin 2 at the BBB.

CONCLUSIONS: By elucidating the complexity of endothelial response to pericyte deficiency at cellular resolution, our study provides insight into the importance of brain pericytes for endothelial arterio-venous zonation, angiogenic quiescence, and a limited set of BBB functions. The BBB-reinforcing role of ANGPT2 (angiopoietin 2) is paradoxical given its wider role as TIE2 (TEK receptor tyrosine kinase) receptor antagonist and may suggest a unique and context-dependent function of ANGPT2 in the brain.

GRAPHIC ABSTRACT: A graphic abstract is available for this article.

Key Words: angiopoietin 2 ■ blood-brain barrier ■ endothelial cells ■ pericyte ■ permeability

Editorial, see p 511 | Meet the First Author, see p 453

Pericytes and vascular smooth muscle cells (VSMCs), collectively referred to as vascular mural cells, form together with the endothelial cells (ECs) the cellular component of the blood vessel wall. While VSMCs surround arteries and veins and, depending on vessel type, regulate vascular tone, and diameter, pericytes are typically embedded within the basement membrane of blood capillaries, where they establish direct contacts with ECs.[1] Pericyte morphology, distribution, and density vary between organs and vascular beds.

Correspondence to: Christer Betsholtz, PhD, Department of Immunology, Genetics, and Pathology, Uppsala University, Dag Hammarskjölds väg 20, SE-751 85 Uppsala, Sweden, Email christer.betsholtz@igp.uu.se; or Maarja A. Mäe, PhD, Department of Immunology, Genetics, and Pathology, Uppsala University, Dag Hammarskjölds väg 20, SE-751 85 Uppsala, Sweden, Email maarja.andaloussi_mae@igp.uu.se

Current address for S. Nordling: Uppsala University, Department of Immunology, Genetics and Pathology, Uppsala, Sweden. Current address for B. Jung: Harvard Medical School, Department of Surgery, Boston, MA.

Current address for Y Zarb: Ludwig-Maximilians-University of Munich, Institute of Physiology, Munich, Germany.

The Data Supplement is available with this article at https://www.ahajournals.org/doi/suppl/10.1161/CIRCRESAHA.120.317473.

For Sources of Funding and Disclosures, see page e60.

Circulation Research is available at www.ahajournals.org/journal/res

Novelty and Significance

What Is Known?

- The blood-brain barrier (BBB) is a semipermeable layer of endothelial cells that selectively regulates solutes crossing into the extracellular fluid of the central nervous system where neurons reside.
- The BBB depends on signals from surrounding nonendothelial cell types, including the pericyte.
- Mice with low numbers of pericytes show increased passage of blood-borne molecules across the BBB.
- Several brain diseases have been associated with pericyte loss or damage and BBB disruption.

What New Information Does This Article Contribute?

- This study provides detailed information about how brain endothelial gene expression is reprogrammed when pericytes are missing.
- The expression of growth factors and proinflammatory mediators is increased, and the molecular profile is shifted from capillary to venous, while the BBB identity remains largely intact.
- Activated angiogenic sprouting without concomitant cell proliferation allowed identification of a specific molecular profile of endothelial tip cells.
- A new mode of BBB impairment induced by pericyte deficiency was uncovered, that is, focal hotspot leakage sites with distinct gene and protein expression including the absence of Angpt2 (angiopoietin 2).
- *Angpt2* null mice show a specific defect in claudin 5-containing tight junctions, suggesting that Angpt2 signaling reinforces endothelial cell-cell contacts when they are challenged by pericyte loss.

Pericytes are obligatory cellular constituents of blood microvessels, but their function(s) remain poorly understood. Pericytes are particularly numerous in the brain and play a poorly defined role in the development and regulation of the BBB. Numerous cerebral diseases have been associated with pericyte loss or damage, but whether this is causally pathogenic or a secondary effect is not clear. Using a mouse model with extensive brain pericyte hypoplasia, we studied how the absence of pericytes influences gene expression and function in brain endothelial cells. We found an extensive endothelial heterogeneity, including specific alterations in the expression of molecular transporters, a venous-shifted identity, the activation of angiogenic sprouting, and 2 distinct modes of BBB disruption, one widespread, involving vesicular transcytosis, and one focal, involving disrupted tight junctions. The latter (hotspot leakage sites) showed lowered expression of Angpt2, which first appeared paradoxical, since Angpt2 is primarily an endothelial destabilizing signal outside of the brain. However, *Angpt2* knockout mice demonstrated disrupted claudin 5-containing tight junctions in the brain, suggesting that Angpt2 is necessary for proper BBB development and that reduced Angpt2 expression triggers BBB disruption when pericytes are missing.

Nonstandard Abbreviations and Acronyms

ANGPT2	angiopoietin 2
ANPEP	aminopeptidase N
A-V	arterio-venous
BBB	blood-brain barrier
BMP	bone morphogenetic protein
CDH5	vascular endothelial cadherin
CLDN5	claudin 5
CNS	central nervous system
CSPG4	chondroitin sulfate proteoglycan 4
CTGF	connective tissue growth factor
EC	endothelial cell
ERG	erythroblast transformation specific-related gene
FACS	fluorescence-activated cell sorting
FGFBP1	fibroblast growth factor-binding protein-1
GFP	green fluorescent protein
ICAM1	intercellular adhesion molecule 1
MFSD2A	major facilitator superfamily domain containing 2
PDGF-B	platelet-derived growth factor-B
PDGFRB	platelet-derived growth factor receptor β
PECAM1	platelet endothelial cell adhesion molecule 1
PLVAP	plasmalemma vesicle-associated protein
scRNAseq	single-cell RNA sequencing
SLC16A1	solute carrier family 16 member 1
TIE2	TEK receptor tyrosine kinase
TFRC	transferrin receptor C
tSpace	trajectory space
VSMCs	vascular smooth muscle cells

The central nervous system (CNS) microvasculature is considered to have a high pericyte density compared with peripheral organs,[2] suggesting a specific importance of pericytes in the CNS. Indeed, studies suggest that pericytes are critically required for the establishment of fully functional blood-brain barrier (BBB) and

blood-retina barrier.[3–6] Developmental absence or reduction of pericytes leads to increased endothelial transcytosis and misexpression of molecular transporters and leukocyte adhesion molecules.[3–7] Several CNS diseases have been associated with pericyte loss or damage, including diabetic retinopathy,[8–10] stroke,[11] Alzheimer disease,[12–14] amyotrophic lateral sclerosis,[15] and aging.[16] However, whether pericyte damage contributes causally, and how and to what extent pericytes regulate the functional state of ECs in the pathogenesis of these conditions, are still not clear.

PDGFB (Platelet-derived growth factor-B) signaling through PDGFRB (PDGF receptor-β) is essential for pericyte recruitment during developmental angiogenesis and postnatal survival in mice.[17,18] Pericyte-deficient adult mice can, however, be generated through partial PDGFB/PDGFRB loss-of-function approaches. The most extensively pericyte-deficient brain microvasculature compatible with adult life observed so far occurs in mice carrying a homozygous deletion of the PDGFB heparan sulfate proteoglycan-binding motif (*Pdgfb*$^{ret/ret}$ mice).[19,20] These mice show increased BBB permeability, dysregulated CNS immune homeostasis, and defective paravascular fluid transport, and they model the human genetic disease primary familial brain calcification.[3,7,21–26] Here, we characterize the EC consequences of pericyte loss in *Pdgfb*$^{ret/ret}$ mice using single-cell RNA sequencing (scRNAseq) in combination with high-resolution imaging and genetic analyses of candidate molecular mediators of permeability changes. Our data show that pericytes regulate EC identity and function in multiple ways. We identify 2 distinct modes of BBB breakdown in *Pdgfb*$^{ret/ret}$ mice and uncover an unexpected role of ANGPT2 (angiopoietin 2) at the BBB. Our data illustrate the power of scRNAseq to decode EC heterogeneity and provide a resource for the further analysis and interpretation of microvascular abnormalities in the adult brain.

METHODS

Data Availability

The data that support the findings of this study are available from the corresponding author upon reasonable request. The single-cell raw sequencing data and also processed counts table of our study are available from the NCBI Gene Expression Omnibus (GSE146007). Previously published wt EC scRNA-seq data set used in this study is also available in the GEO repository (GSE98816).

A complete description of the methods and reagents is provided in the Data Supplement.

RESULTS

A Major Proportion of the *Pdgfb*$^{ret/ret}$ Cortical Microvasculature Is Devoid of Pericyte Contact

Constitutive *Pdgfb* knockout mice (*Pdgfb*$^{-/-}$) die perinatally displaying >95% loss of brain pericytes.[17,27] By comparison, *Pdgfb*$^{ret/ret}$ mice[19] show 70% to 80% brain pericyte loss and survive postnatally (Figure 1A).[3] EC hyperplasia was reported in *Pdgfb*$^{-/-}$ embryos,[28] but we concluded that overall EC numbers were normal in the adult *Pdgfb*$^{ret/ret}$ brain using immunofluorescent staining of EC nuclei by ERG (erythroblast transformation specific-related gene) antibodies (Figure IA in the Data Supplement). However, ECs formed a sparser network of vessels with increased diameter and numbers of ECs per vessel length in these mice (Figure 1A insets a and b and Figure IB in the Data Supplement).

We found numerous angiogenic sprouts with distinct tip cells[29] in adult *Pdgfb*$^{ret/ret}$ brains, whereas these were rarely seen in age-matched wild type (*Pdgfb*$^{+/+}$) or heterozygous (*Pdgfb*$^{ret/+}$) controls (Figure 1A inset c). By immunofluorescent staining for ERG and PECAM1 (platelet endothelial cell adhesion molecule 1), we calculated the tip cell frequency to ≈0,6% of the total EC number in *Pdgfb*$^{ret/ret}$ brain (Figure 1B). Labeling with ethynyl deoxyuridine showed that the tip cells were not cycling (Figure IC and ID in the Data Supplement), confirming previous observations in the developing mouse retina.[29] Neither overall cell proliferation, nor EC proliferation or death, the latter judged by cleaved caspase-3 immunofluorescent staining, were significantly increased in *Pdgfb*$^{ret/ret}$ cerebral cortex (Figure ID and IE in the Data Supplement). The unchanged turnover of ECs suggests that the observed angiogenic sprouting in *Pdgfb*$^{ret/ret}$ brains is either abortive (sprouts fail to establish patent capillary connections) or reflects a balanced formation and regression of vessel branches.

To assess pericyte morphology and density, we used immunofluorescent analysis for ANPEP (aminopeptidase N) and 2 transgenic reporters: chondroitin sulfate proteoglycan 4 promoter-driven dsRED (*Cspg4*-dsRED) and PDGFRB promoter-driven GFP (green fluorescent protein) (*Pdgfrb*-GFP)[30,31] in combination with Hoechst nuclear staining and EC detection by immunofluorescent staining for ERG and PECAM1. These analyses showed that while residual pericyte in *Pdgfb*$^{ret/ret}$ was elongated, the pericyte:EC ratio in *Pdgfb*$^{ret/ret}$ cerebral cortex was ≈8-fold lower than in *Pdgfb*$^{ret/+}$ littermates (1:54 versus 1:7; Figure 1C through 1E) and >10-fold lower than separately bred *Pdgfb*$^{+/+}$ mice, where the pericyte:EC ratio was estimated to 1:4. The slight reduction in pericyte density in *Pdgfb*$^{ret/+}$ compared with *Pdgfb*$^{+/+}$ does not correlate with any obvious differences in vascular

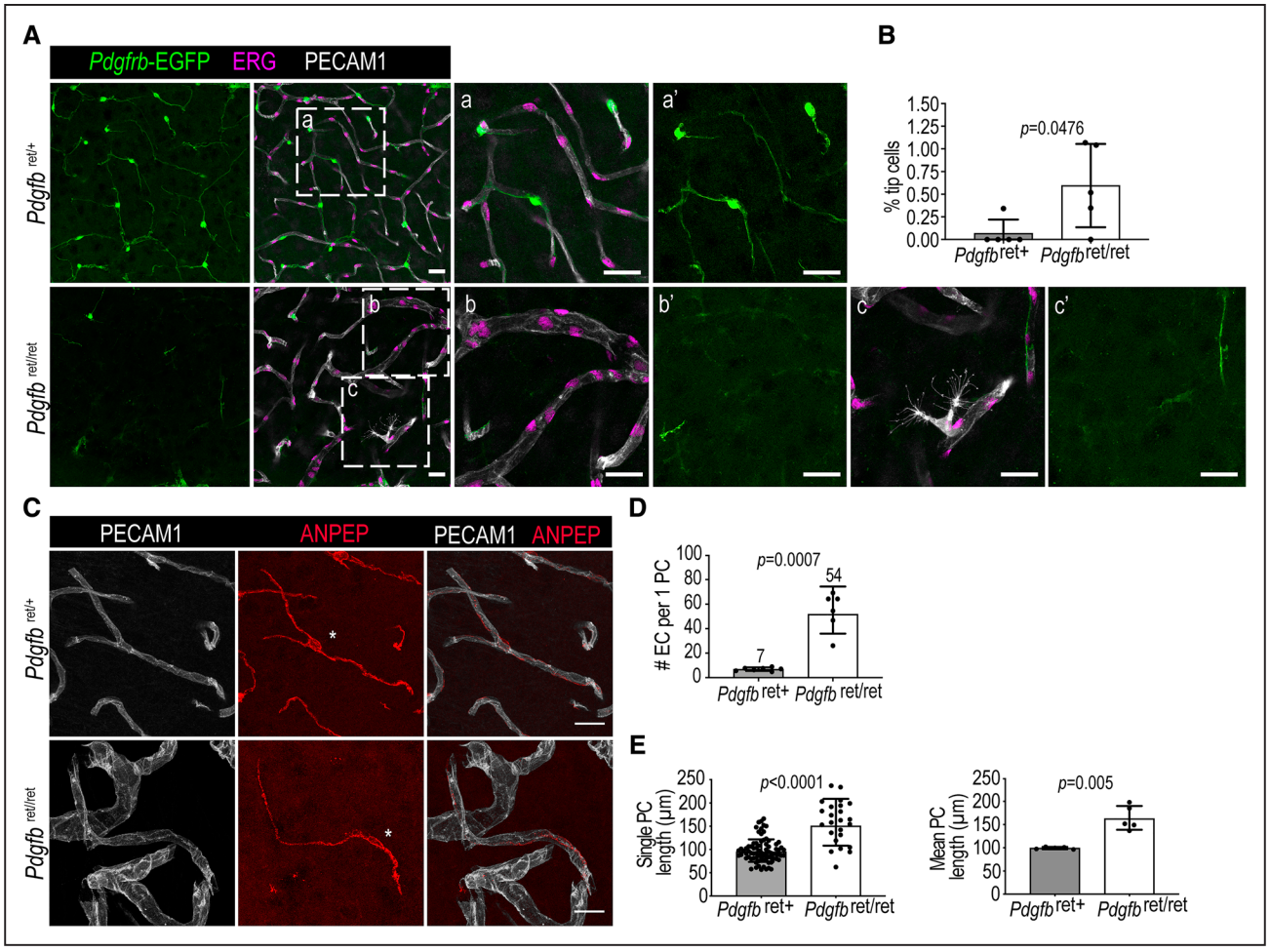

Figure 1. Vascular abnormalities in Pdgfb$^{ret/ret}$ mice.
A, Immunofluorescent (IF) and *Pdgfrb*-EGFP analysis of sagittal sections from adult brain cortex. Insets a–c illustrate vascular morphologies and cellular composition. Scale bars 25 µm. **B**, Quantification of tip cells per field as percentage of the total endothelial cell (EC) number (n=5, 6 fields per mouse). **C**, Representative confocal images of pericyte (PC) IF, asterisk marks the cell soma. Scale bar 20 µm. **D**, Quantification of PC:EC ratio (*Pdgfb*$^{ret/+}$ n=7 and *Pdgfb*$^{ret/ret}$ n=6, 6 fields per mouse). **E**, Quantification of PC length in cerebral cortex. **Left** graph illustrates the length range in all measured PC (n=5 mice, *Pdgfb*$^{ret/+}$ n=78 PC and *Pdgfb*$^{ret/ret}$ n=24 pericytes). **Right** graph shows mean PC length per mouse (n=5). **D** and **E**, Data were normally distributed and significance evaluated using unpaired 2-tailed *t* test with Welch correction. **B**, **D**, Data were unevenly distributed and significance evaluated using nonparametric Mann-Whitney *U* test. **B** and **D**, The data are presented as geometric mean ± geometric SD, and in **B**, as mean±SD. ANPEP indicates aminopeptidase N; ERG, erythroblast transformation specific-related gene; and PECAM1, platelet endothelial cell adhesion molecule1.

morphology and function, however, according to our previous analyses.[3]

Pdgfb$^{ret/ret}$ capillaries with residual pericyte contact showed a normalized diameter (Figure 1C), suggesting a direct effect of pericytes on capillary diameter. While in *Pdgfb*$^{ret/ret}$ each pericyte contacted an extended capillary length, a major proportion (≈75%) of the capillary length remained devoid of visible pericyte contact. In contrast, both *Pdgfb*$^{ret/+}$ and wild-type mice showed pericyte contact along ≈100% of the brain capillary vessel length (Figure 1A), confirming previous observations.[32]

Although less severely than pericytes, also VSMCs were affected in *Pdgfb*$^{ret/ret}$ brains. *Pdgfb*$^{ret/ret}$ arteries and veins maintain VSMCs coverage, but we observed a reduction in the α-smooth muscle actin (a.k.a) staining of larger arteries (Figure IF in the Data Supplement), as well as a shift from circumferential to longitudinal orientation and reduced vessel coverage by VSMC at these sites.

Endothelial Transformation and Skewed Arterio-Venous Zonation in *Pdgfb*$^{ret/ret}$ Mice

We applied scRNAseq analysis using fluorescence-activated cell sorting (FACS) and the SmartSeq2 protocol[33] to investigate how pericyte deficiency affects EC gene expression. We first generated *Pdgfb*$^{ret/+}$ and *Pdgfb*$^{ret/ret}$ mice carrying *claudin 5* (*Cldn5*)-GFP and *Cspg4*-DsRed, transgenic reporters for EC and pericyte, respectively.[31,34] mRNA contamination between ECs and pericytes is frequently observed in public scRNAseq data sets,[35,36] likely reflecting that the 2 cell types, firmly adjoined by a common basement membrane, are difficult to separate during

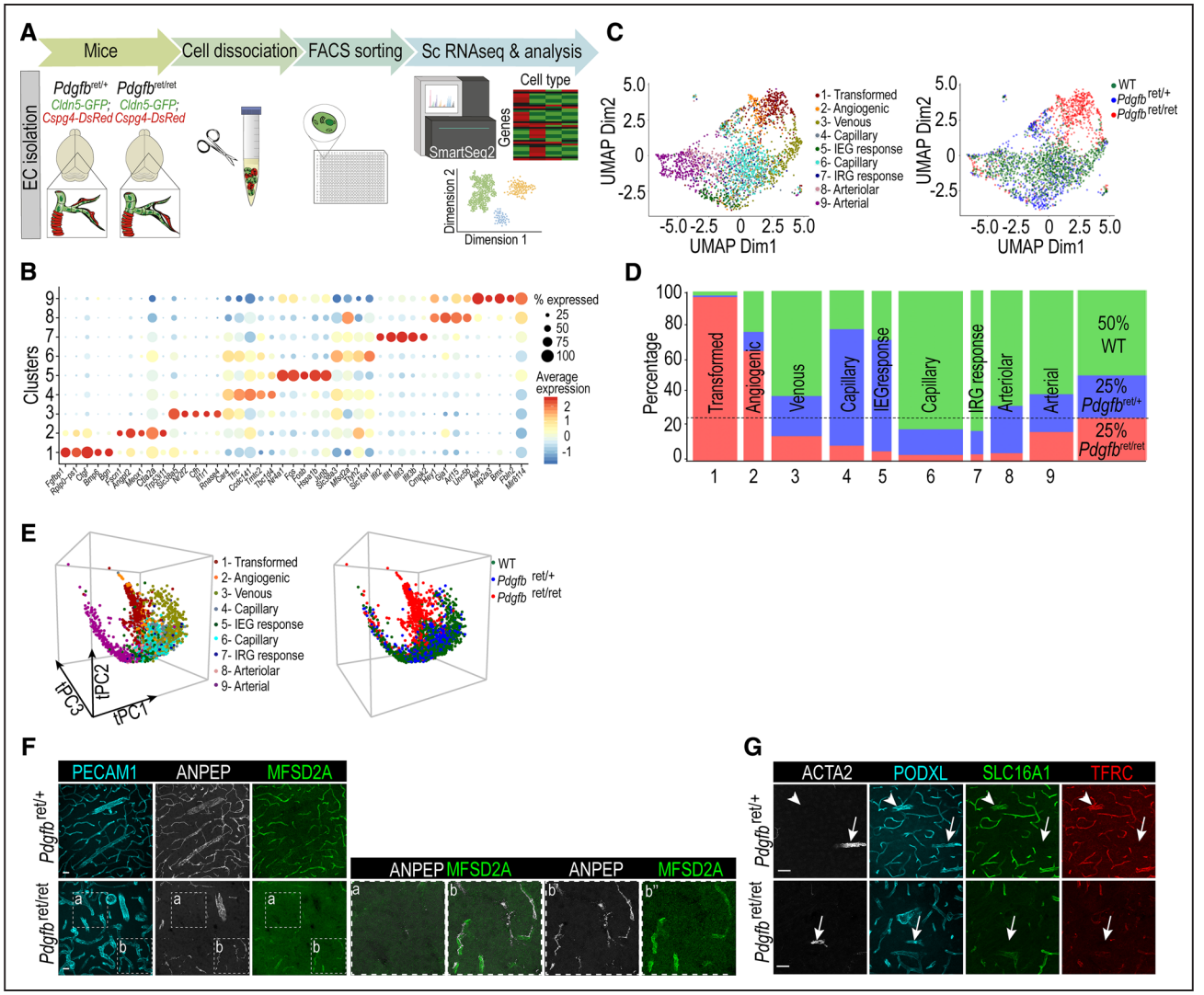

Figure 2. Transcriptomic changes in endothelial cell (EC) devoid of pericyte (PC) contact.
A, Schematic overview of EC isolation for single-cell RNA sequencing (scRNAseq). **B**, Dot plot of top markers for 9 Pagoda2 EC clusters. Dot size illustrates percentage of cells presenting transcript sequence count(s) and color illustrates the average expression level in the cells within a cluster. **C**, The 9 EC clusters from **B** visualized in a uniform manifold approximation and projection (UMAP) landscape (**left**), UMAP distribution by genotype (**right**). **D**, Genotype proportions in each cluster. Total proportion is shown in the **right** column. **E**, Trajectory space (tSpace) projections of all EC labeled by cluster assignment (**left**) and genotype (**right**). **F** and **G**, Immunofluorescent (IF) analysis of arterio-venous (A-V) marker expression as indicated. **F** inset a illustrates that EC devoid of PC lack MFSD2A (major facilitator superfamily domain containing 2) expression. Inset b shows that EC with residual PC contact retain MFSD2A expression. Scale bar 25 μm. **G**, IF staining against the capillary/venous markers SLC16A1 (solute carrier family 16 member 1) and TFRC (transferrin receptor C). PODXL (podocalyxin-like) stains all EC. Arrowheads point to veins and arrows to arterioles. Scale bar 40 μm.

tissue disintegration. We, therefore, used the double transgenic reporters to deselect contaminated cells during FACS.[37] Pure brain EC (*Cldn5*-GFP$^+$, *Cspg4*-DsRed$^-$) from 3-month-old mice were sorted into 384-well-plates and RNA sequenced (Figure 2A).

One thousand one hundred eighty-seven quality-controlled single-cell transcriptomes from *Pdgfb*$^{ret/+}$ and *Pdgfb*$^{ret/ret}$ mice were obtained and compared with scRNAseq data reported previously from wild-type mice of the same genetic background.[34,37] A total of 2389 EC transcriptomes distributed into 9 clusters using the Pagoda2 package (Figure 2B).[38] Based on previously established markers for arterio-venous (A-V) zonation in the adult mouse brain,[34] some clusters were identified as arterial/arteriolar (nos. 8 and 9), capillary (nos. 4 and 6), or venous (no. 3) EC (Figure 2C). Gene ontology analysis of cluster-enriched transcripts showed significantly different association with terms for biological processes such as vascular development (cluster no. 9), cell migration (cluster no. 8), molecular transport (cluster no. 6), and cell adhesion (cluster no. 3) implying functional differences related to A-V position (Figure IIA and Table I in the Data Supplement). Two clusters (nos. 5 and 7) were characterized by high expression of immediate

early genes and interferon response genes, respectively, and the enriched transcriptomes of these 2 clusters were associated with gene ontology terms encompassing metabolic processes (no. 5) and response to virus (no. 7), respectively (Figure IIA and Table I in the Data Supplement). We consider it likely that the immediate early genes response was established during the experimental procedure as a result of cell stresses induced by tissue digestion. While we do not have an explanation for the underrepresentation of *Pdgfb*$^{ret/ret}$ cells in the interferon response genes cluster, it is possible that it is caused by stochastic exposure to double-stranded RNA released from lysed cells.[34,39,40] Similar clusters have been observed in scRNAseq data sets from other organs,[41] and they will not be discussed further herein. Finally, 2 clusters were enriched with transcripts that encode proteins associated with angiogenesis (no. 2) and growth factor signaling (no. 1). Because cluster number 1 represents the strongest deviation from normal, we named this cluster transformed. The enriched transcriptomes of both clusters numbers 1 and 2 were associated with gene ontology terms for developmental processes and cell migration (Figure IIA and Table I in the Data Supplement), similar to the arterial cluster number 9 in spite of differences in clustering and specific gene expression (see further below).

In a uniform manifold approximation and projection landscape, the arterial/arteriolar and venous clusters were located at opposite ends, separated by the capillary/venular clusters (Figure 2C). The transformed and angiogenic clusters (nos. 1 and 2) were on the side of this trajectory but closer to the capillary-venous clusters. The relative distribution of cells of the 3 genotypes (*Pdgfb*$^{ret/ret}$, *Pdgfb*$^{ret/+}$, and *Pdgfb*$^{+/+}$) in the different clusters showed that cluster number 1 was almost completely composed of, and cluster number 2 dominated by, *Pdgfb*$^{ret/ret}$ cells (Figure 2C and 2D and Figure IIB in the Data Supplement). Conversely, the microvascular clusters (capillaries nos. 4, 6 and arterioles no. 8) were underrepresented with *Pdgfb*$^{ret/ret}$ cells (Figure 2D). The contribution of *Pdgfb*$^{ret/ret}$ cells to the arterial and venous clusters was instead roughly proportional to their overall representation in the data set (≈25%), suggesting that the arterial and venous EC phenotypes remain comparably intact in the *Pdgfb*$^{ret/ret}$ brain (Figure 2D). Capillary EC distributed into 2 clusters (nos. 4 and 6) with different proportions of *Pdgfb*$^{ret/+}$ and *Pdgfb*$^{+/+}$ cells, however, with similar marker expression and position in uniform manifold approximation and projection landscape (Figure 2B and 2C). The cluster numbers 4 versus 6 assignment may, therefore, reflect a technical batch effect or minor quantitative gene expression differences provided by the 2 control genotypes. The most differentially expressed genes for each cluster are shown in Figure 2B. Lists of enriched genes for clusters numbers 1 to 9 are provided in Table II in the Data Supplement. The gene expression patterns of all genes across the clusters are available gene-by-gene as bar-plot data at https://betsholtzlab.org/Publications/RetECscRNAseq/database.html.

To define nearest neighbor relationships between cells, we next applied trajectory space (tSpace) analysis, which recapitulates dynamic and spatial relationships better than uniform manifold approximation and projection landscape in multiple organisms and processes.[42–44] tSpace defined 3 principal branches in our data, representing arterial, venous, and angiogenic ECs, all joined by a centrally located population of capillary/microvascular cells (Figure 2E). The tSpace branches correspond roughly to the different corners of the uniform manifold approximation and projection landscape but provide clearer separation of mature versus transformed/angiogenic subsets of EC.

Taken together, these analyses suggest that a major proportion (albeit not all) of the *Pdgfb*$^{ret/ret}$ brain microvascular ECs display a substantially transformed gene expression. In addition to the upregulated expression of molecules involved in angiogenesis and growth factor signaling, the cells of clusters numbers 1 and 2 show decreased expression of certain transporters (*Mfsd2a*, *Tfrc*, *Slc16a1*, and *Slc38a3*; (Figure 2B), suggesting that pericyte contact is required for ECs to assume and/or maintain certain specific BBB functions. Nevertheless, the phenotypic transformation of EC that we observe in the absence of pericytes does not reflect a general loss of BBB markers. Many established BBB markers, including the tight junction molecule *Cldn5*, the glucose transporter Glut 1 (*Slc2a1*), other influx transporters (*Slco1c1*, *Slco1a4*, and *Slc40a1*), efflux transporters (*Abcb1a* a.k.a. P-glycoprotein) and the BBB-specific transcription factor *Zic3*, were all normally expressed (Figure III in the Data Supplement). Out of 64 CNS-specific EC markers[45] regulated by Wnt,[46] 20 were downregulated and 2 upregulated in *Pdgfb*$^{ret/ret}$ cells (Table III in the Data Supplement), but these changes were modest (2-fold or less). Moreover, upregulation and downregulation, respectively, of venous (*Slc38a5* and *Nrp2*) and capillary (*Mfsd2a*, *Slc16a1*, and *Slc1a1*) markers[34] suggested venous skewing of the EC identity rather than loss of BBB functions (Figure IVA in the Data Supplement). To deepen the analysis of A-V zonation, we assessed 64 top venous and arterial markers of brain ECs[34] across the 9 clusters, confirming that *Pdgfb*$^{ret/ret}$ ECs are venous-shifted with several venous markers upregulated including *Nr2f2* and intercellular adhesion molecule 1 (*Icam1*; Figure IVB in the Data Supplement). Although less conspicuously, some arterial markers were also upregulated, including *Bmx* and *Gkn3*, possibly suggesting a mixed A-V identity in the *Pdgfb*$^{ret/ret}$ microvasculature (Figure IVC in the Data Supplement).

To confirm the aberrant marker expression and disturbed A-V zonation in the *Pdgfb*$^{ret/ret}$ brain vasculature at the tissue level, we analyzed protein and transgenic reporter expression (Figure 2F and 2G and Figure IIC

and IID in the Data Supplement). Combined MFSD2A (major facilitator superfamily domain containing 2)[34,47] and ANPEP[34,48] immunofluorescent analysis showed that MFSD2A was lost specifically in EC devoid of pericyte contact (Figure 2F), suggesting that pericytes control EC expression of MFSD2A directly through paracrine or juxtacrine signals. This conclusion was also supported by *Mfsd2a*-CreERT2-induced Ai9 reporter[49] expression, which labeled 84% of the capillary length in controls compared with 32% in *Pdgfb*$^{ret/ret}$ (Figure IIC and IID in the Data Supplement). Similarly, expression of the capillary-venous markers SLC16A1 (solute carrier family 16 member 1) and TFRC (transferrin receptor C)[3,34] were focally lost in *Pdgfb*$^{ret/ret}$ brain microvessels (Figure 2G). Taken together, scRNAseq and tissue imaging show disturbed EC differentiation and A-V zonation in the *Pdgfb*$^{ret/ret}$ brain, implicating a critical role for pericyte in the establishment of proper vascular hierarchy in this organ.

Endothelial Heterogeneity Hallmarks the *Pdgfb*$^{ret/ret}$ Microvasculature

We next focused our attention to the cells of the transformed and angiogenic clusters (nos. 1 and 2) dominated by *Pdgfb*$^{ret/ret}$ cells. A comparison between all *Pdgfb*$^{ret/ret}$ and all control (*Pdgfb*$^{ret/+}$ and *Pdgfb*$^{+/+}$) cells revealed almost 1000 differentially expressed genes (Table IV in the Data Supplement; the top 25 upregulated or downregulated genes are shown in Figure V in the Data Supplement). Although a few cells in clusters number 1 and 2 originated from *Pdgfb*$^{ret/+}$ and *Pdgfb*$^{+/+}$ controls, the *Pdgfb*$^{ret/ret}$ cells distinguished from these by being uniquely enriched with a number of transcripts, including fibroblast growth factor-binding protein-1 (*Fgfbp1*), connective tissue growth factor (*Ctgf*), bone morphogenetic protein (*Bmp*) *-4* and *-6* and *Angpt2* (Figure 3A). Intriguingly, high expression of these genes was seen also in the *Pdgfb*$^{ret/ret}$ cells present in the venous (no. 3) and capillary (no. 4) clusters (Figure 3A). *Fgfbp1* encodes a secreted protein that binds FGFs (fibroblast growth factors) and promotes signaling through FGFRs,[50,51] and it has been functionally implicated in embryonic angiogenesis in the chick[52] and BBB development in the mouse.[53] *Fgfbp1* expression is high in mouse embryonic brain EC (our unpublished data) but negligible in adult brain EC.[34,36] Our results, therefore, suggest that the absence of pericyte causes a molecular transformation of capillary EC, including loss of markers for brain capillary specialization and concomitant gain of venous markers, as well as upregulation of transcripts normally expressed during development (*Fgfbp1*) or in pathological angiogenesis (*Angpt2*).

To explore the putative heterogeneity of the cells of clusters number 1 and 2, we reclustered them into 5 subclusters (i-v in Figure 3B). Subcluster i, comprising 90 cells, showed expression of several genes proposed as markers for tip cells, including *Mcam* and *Angpt2* (Figure 3C).[36,54–57] It also contained *Lamb1*-positive cells. Immunofluorescent analysis of MCAM (melanoma cell adhesion molecule) and LAMB1 (laminin subunit beta 1) confirmed the specific expression of these 2 proteins in tip cells (Figure 3D). MCAM is expressed also by pericytes[1] but at substantially lower level compared with tip cells (Figure 3D).

Not all cells in subcluster i were *Mcam* and *Lamb1* positive. To assess putative further heterogeneity in subcluster i, we sorted the transcriptomes unidimensionally using the sorting points into neighborhoods algorithm,[58] resulting in 2 groups, i-1 and i-2, consisting of 7 and 83 cells, respectively (Figure 3E). i-1 matched the expected tip cell profile, including expression of *Mcam* and *Lamb1* along with previously suggested tip cell markers *Cxcr4*,[56] *Pgf*,[59] *Kcna5*, *Sirpa*, and *Smoc2*.[45] Gene ontology analysis of i-1 markers showed association with actin filament assembly and filopodia (Figure 3F) as expected for tip cells.[29] The number of i-1 cells constituted 1.2% of the total number of analyzed *Pdgfb*$^{ret/ret}$ EC, that is, roughly comparable to the tip cell frequency counted in *Pdgfb*$^{ret/ret}$ brain (0.6%).

Subcluster ii was enriched with capillary markers[34] (eg, *Mfsd2a* and *Tfrc*) and dominated by *Pdgfb*$^{ret/ret}$ cells (Figure 3C). Subclusters iii and iv were enriched for venous markers[60] (eg, *Nr2f2* and *Bmp4*) with iv displaying immediate early genes on top (Figure 3B), presumably reflecting gene activation during tissue dissociation, as discussed above. Subcluster v was positive for arteriolar EC markers[60] (*Gja4*, *Bmx*, *Gkn3*, and *Sema3g*; Figure 3B). Thus, the EC heterogeneity revealed through subcluster analysis appears to reflect in part a shadow A-V identity among the angiogenic and transformed ECs present in *Pdgfb*$^{ret/ret}$ brain. For complete lists of enriched genes for each subcluster, see Table V in the Data Supplement.

As a complement to the supervised assignment of A-V shadow identity using selected A-V marker distribution in subclusters, we also analyzed the relationships between subclusters i-v and their mature counterparts (global clusters number 3–9) using unsupervised mutual nearest neighbor alignment[61] and visualization in tSpace (Figure 3G through 3J and Figure VIA and VIB in the Data Supplement). Mutual nearest neighbor alignment provides batch correction, that is, it subtracts global differences between genotypes, such as *Fgfbp1* and other genes hallmarking the *Pdgfb*$^{ret/ret}$ batch (Figure 3G and 3H). With this analysis, the transformed arterial cells stayed at more proximal locations in the arterial tSpace branch (weaker shadow identity) compared with the transformed venous cells, which distributed more distally into the venous branch (stronger shadow identity; Figure VIA in the Data Supplement). The angiogenic ECs were still positioned within their own branch after mutual nearest neighbor alignment, with cluster i-1 cells (tip cells) preferably at distal position (Figure 3I and 3J and Figure VIB in the Data Supplement). In conclusion, both supervised cluster annotation (Figure 3C) and

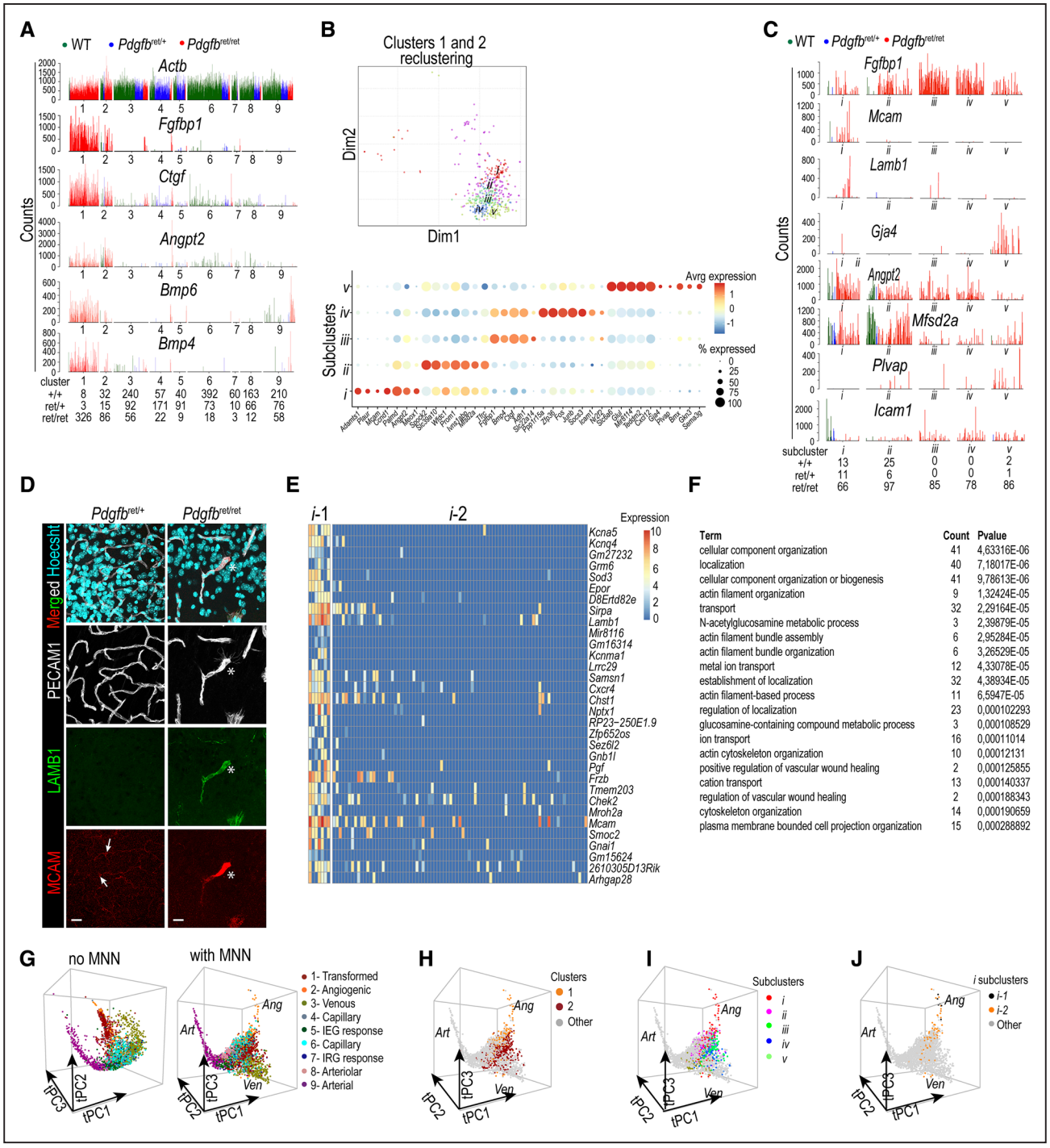

Figure 3. Pdgfb$^{ret/ret}$ endothelial cell (EC) heterogeneity.

A, Single-cell RNA sequencing (ScRNAseq) bar plots showing the expression of selected genes that are upregulated in clusters number 1 and 2. **B**, **Upper**: Reclustering of number 1 and 2 results in 5 subclusters (i-v). **Lower**: Dot plot showing enriched genes for subclusters i-v. Dot size illustrates percentage of cells presenting transcript sequence count(s) and color illustrates the average expression level in the cells within a cluster. **C**, Bar plots of representative markers for each subcluster. **D**, Immunofluorescent (IF) visualization of tip cell (asterisk) in cerebral cortex. Arrows point at low-MCAM (melanoma cell adhesion molecule) expressing pericyte (PC). Scale bar 20 μm. **E**, Heatmap of i-1-enriched markers across i-1 and i-2 cells sorted by sorting points into neighborhoods (SPIN). **F**, Gene ontology (GO) analysis of subcluster i-1-enriched genes. Terms for biological process are shown. **G**–**J**, Trajectory space (tSpace) projections. **G**, Supervised (**left**) and unsupervised (**right**) mutual nearest neighbor (MNN) alignment of EC by clusters. **H**–**J**, Cell distribution and gene expression in MNN-aligned graphs, as indicated. Ang indicates angiogenic; Art, arterial; and Ven, venous.

unsupervised mutual nearest neighbor alignment (Figure 3G through 3J and Figure VIA and VIB in the Data Supplement) suggested a heterogenous A-V shadow identity with venous preference among the transformed EC, and the presence of angiogenic EC with a distinguishable tip cell transcriptome.

Endothelial Phenotypes Correlate With BBB Dysfunction

The BBB leakage observed in *Pdgfb*$^{ret/ret}$ appears to be caused, in part, by endothelial transcytosis.[3] Systemically administered tracers between 1 and 200 kDa in size accumulate progressively in the *Pdgfb*$^{ret/ret}$ brain over 2 to 16 hours.[3] This accumulation is, however, uneven across the brain, which might reflect local differences in residual pericyte contact and different modes of BBB impairment in different vessel types along the A-V axis. We, therefore, set out to explore the correlation between gene expression and BBB dysfunction, focusing on subclusters iii, iv, and v, which were dominated by ECs from *Pdgfb*$^{ret/ret}$ (Figure 3C). ANGPT2 is known to destabilize blood vessels through its antagonistic function at the tyrosine kinase receptor TIE2 (reviewed in Augustin et al[62]). MFSD2A, however, has a BBB-stabilizing role (its loss leads to increased brain endothelial transcytosis[63,64]). We, therefore, anticipated that subclusters iii and iv, in which *Angpt2* was high and *Mfsd2a* low, represented the ECs with the most extensively impaired BBB. However, by correlating the leakage of systemically administered 70 kDa tetramethylrhodamine-dextran with ANGPT2 and MFSD2A expression in tissue sections, we instead found that the most extensive (hotspot) tetramethylrhodamine-dextran leakage occurred at sites where both ANGPT2 and MFSD2A were low, that is, corresponding to the gene expression pattern of subcluster v (Figure 3C). Thus, in addition to a broadly observable vesicular accumulation of tetramethylrhodamine-dextran (Figure 4A) in ECs, consistent with transcytosis,[3] we detected hotspot leakage sites (Figure 4B). Neither type of leakage was observed in controls. Whereas areas with detectable transcytosis displayed MFSD2A expression (Figure 4A), only about 10% of the hotspot leakage sites had detectable MFSD2A (Figure 4B and 4C). ANGPT2 was barely detectable by immunofluorescent staining in control brains, but strongly and heterogeneously expressed in *Pdgfb*$^{ret/ret}$ vessels, including but not limited to tip cells (Figure 4A and 4B). However, ANGPT2 was low or undetectable at most hotspot leakage sites (Figure 4B), and conversely, most sites with high ANGPT2 staining did not display hotspot leakage (Figure 4B). Quantifications revealed that only ≈11% of the hotspot leakage sites showed detectable ANGPT2 (Figure 4C). ANGPT2 expression was mainly observed in vessels devoid of mural cells, suggesting that it depends on local rather than systemic cues (Figure 4D). PLVAP (Plasmalemma vesicle-associated protein) was upregulated at the mRNA level (*Plvap*) in *Pdgfb*$^{ret/ret}$ brains in subcluster *v* cells (Figure 3C) and an irregular PLVAP staining could be detected at a majority (59%, Figure 4C) of the hotspot leakage sites (Figure 4E). PLVAP is normally found in fenestrated blood vessels, including the capillaries of the brain's circum-ventricular organs, as exemplified by the organum vasculosum of the lamina terminalis and choroid plexus in the lateral ventricle, but otherwise not in the healthy BBB (Figure VIIA in the Data Supplement). Additionally, the leukocyte adhesion molecule, *Icam1* mRNA was upregulated in the *Pdgfb*$^{ret/ret}$ dominated subclusters iii, iv, and v (Figure 3C), a finding supported by ICAM1 protein detection by immunofluorescent staining. In adult control brain, ICAM1 was detectably expressed mainly in veins and arteries (Figure 4F and data not shown), whereas in *Pdgfb*$^{ret/ret}$, it was broadly upregulated in pericyte-deficient capillaries (Figure 4F and Figure VIIB and VIIC in the Data Supplement). ICAM1 staining was observed at most (92%, Figure 4C) of the hotspot leakage sites. We also found extravasated CD45-positive leukocytes in *Pdgfb*$^{ret/ret}$ brains (but not in controls) often clustered at hotspot leakage sites (Figure VIID in the Data Supplement). Finally, we observed abnormal and irregular patterns of the adherens and tight junction proteins CDH5 (VE-cadherin) and CLDN5 at hotspot leakage sites devoid of mural cells (Figure 4G and 4H), suggesting that EC junctions are altered at these sites.

Collectively, these results suggest 2 distinct modes of BBB dysfunction in *Pdgfb*$^{ret/ret}$. On the one hand, hotspot leakage sites devoid of pericyte clearly visible by 70 kDa tetramethylrhodamine-dextran extravasation; these sites were characterized by an arteriolar EC expression profile (subcluster v in Figure 3C), disturbed junctions, low or missing expression of MFSD2A, upregulated ICAM1 expression, extravasation of leukocytes, and ectopic PLVAP expression. On the other hand, the previously characterized increase in vesicular transcytosis across the EC in *Pdgfb*$^{ret/ret}$ brain[3]; this activated transport leads to widely distributed tracer leakage in *Pdgfb*$^{ret/ret}$ brains and seem to correlate with increased expression of a large number of mRNAs and proteins, including *Fgfbp1*, *Ctgf*, *Angpt2*, and *Bmp4*.

To provide mechanistic insight into the BBB leakage in *Pdgfb*$^{ret/ret}$ brain, we chose *Mfsd2a, Fgfbp1,* and *Angpt2* for further functional interrogation using reverse genetics. *Mfsd2a* was selected for study because it was downregulated in transformed EC in *Pdgfb*$^{ret/ret}$ and has been shown to suppress EC transcytosis in the intact BBB.[63,64] *Fgfbp1* was selected because it is the most strongly upregulated gene in *Pdgfb*$^{ret/ret}$ brain EC and has previously been implicated in BBB regulation.[52,53] *Angpt2*, finally, was selected because it is upregulated in *Pdgfb*$^{ret/ret}$ transformed EC and is known to enhance vascular permeability by antagonizing ANGPT1 signaling through TIE2.[62]

Loss of *Mfsd2a* or *Fgfbp1* Do Not Mediate Major BBB Permeability in *Pdgfb*$^{ret/ret}$ Mice

We compared the distribution of 2 tracers with different sizes, 1 kDa Alexa Fluor 555-(A555)-cadaverine (Figure 5A and 5B) and 70 kDa tetramethylrhodamine-dextran

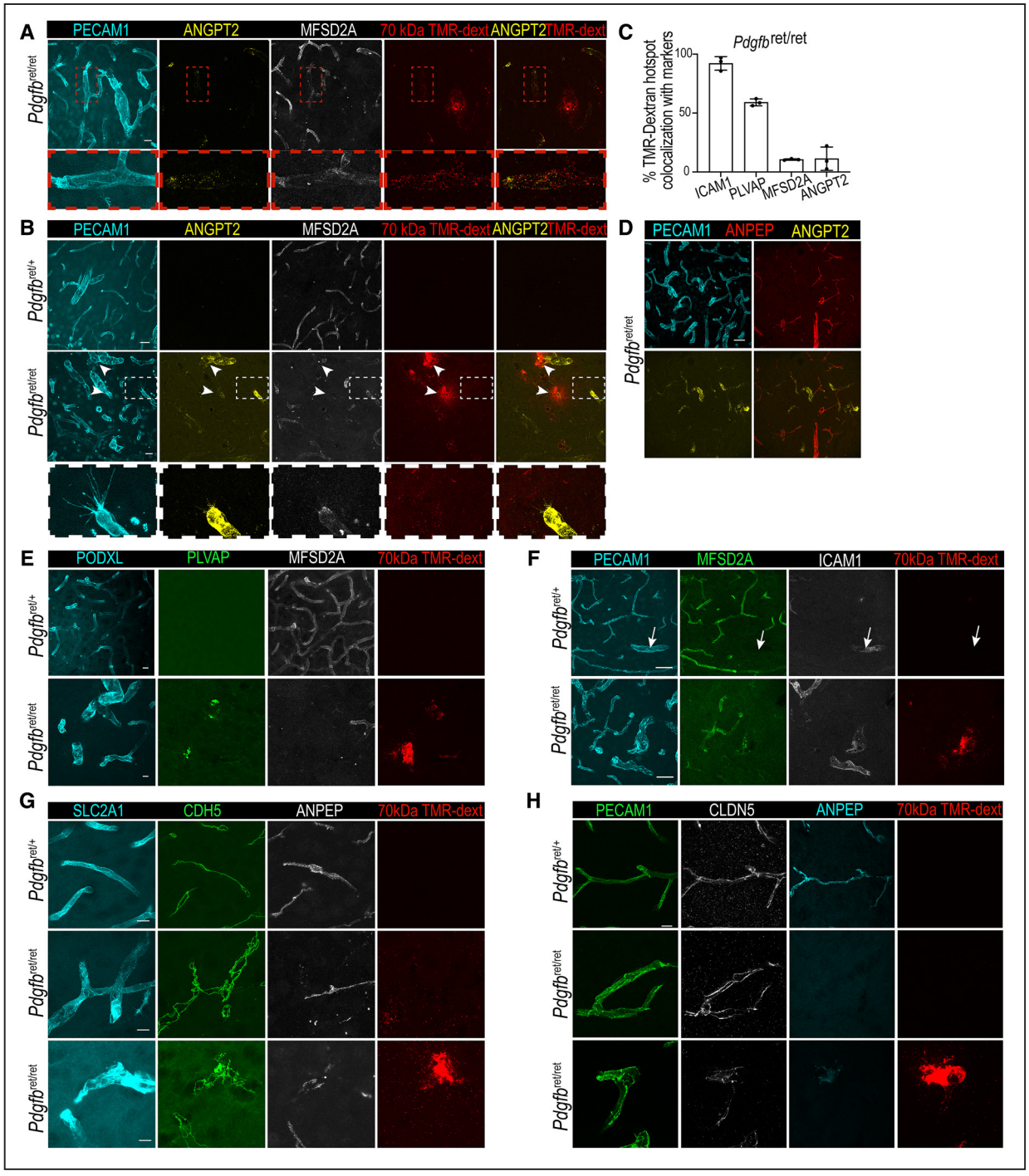

Figure 4. Hotspot leakage sites in Pdgfb$^{ret/ret}$ brains.

A and **B**, Confocal images of cerebral cortex of 70 kDa tetramethylrhodamine (TMR)-dextran (red) injected mice, together with immunofluorescent (IF) staining for the indicated proteins **A**, Inset depicts MFSD2A^{low} vasculature with increased TMR-dextran positive vesicles (transcytosis). Scale bar 20 μm. **B**, Examples of TMR-dextran positive hotspot permeability sites (arrowheads). Inset shows ANGPT2 (angiopoietin 2)-positive tip cell negative for TMR-dextran. Scale bar 20 μm. **C**, Quantification of colocalization between TMR-dextran hotspots and indicated markers (n=3). **D**, Upregulated ANGPT2 expression where pericyte (PC) contact is absent. Scale bar 40 μm. **E**, Illustration of PLVAP (plasmalemma vesicle-associated protein) staining at TMR-dextran positive hotspot permeability sites. Scale bar 20 μm. **F**, The majority of TMR-dextran positive hotspot permeability sites are MFSD2A (major facilitator superfamily domain containing 2)-negative and ICAM1 (intercellular adhesion molecule 1)-positive. Scale bar 40 μm. **G**, Adherens junctions stained for CDH5 are thin and regular in controls (all endothelial cell [EC] stained by anti-SLC2A1 [glucose transporter type 1]) but discontinuous and irregular at TMR-dextran positive hotspot leakage sites. Adherens junctions at nonhotspot permeability sites are irregular but continuous (**middle**). ANPEP (aminopeptidase N) visualizes PC. Scale bar 10 μm. **H**, Tight junctions visualized using anti-CLDN5 (claudin 5) staining are continuous in *Pdgfb*$^{ret/+}$ (all EC visualized by anti-PECAM1 [platelet endothelial cell adhesion molecule 1]) but discontinuous and irregular at TMR-dextran positive hotspot leakage sites. Tight junctions in nonhotspot leakage sites in *Pdgfb*$^{ret/ret}$ are continuous (**middle**). Scale bar 10 μm.

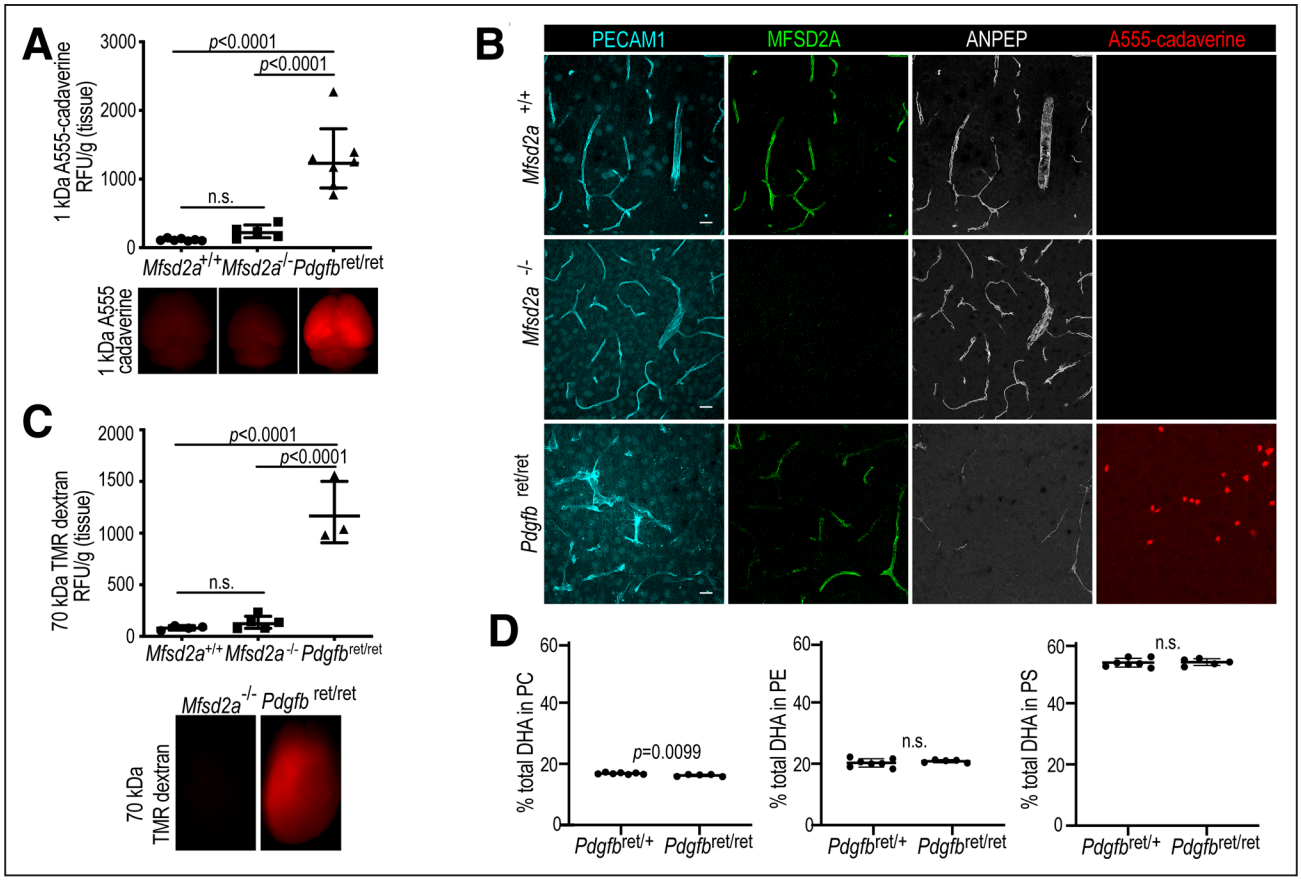

Figure 5. Lack of role of Mfsd2a and Fgfbp1 in Pdgfb$^{ret/ret}$ blood-brain barrier (BBB) leakage.
A and **B**, Intravenously administered 1 kDa Alexa Fluor (A555) cadaverine permeability after 2 h circulation in adult *Mfsd2a*$^{+/+}$, *Mfsd2a*$^{-/-}$ and *Pdgfb*$^{ret/ret}$ mice. **A**, Graph shows quantification of extravasated tracer in the brain (*Mfsd2a*$^{+/+}$ n=7, *Mfsd2a*$^{-/-}$ n=5, and *Pdgfb*$^{ret/ret}$ n=7). **Lower** shows whole brains photographed after tracer circulation. **B**, Three-dimensional reconstructions of confocal image z-stacks of cerebral neocortex vasculature immunofluorescent (IF) stained as indicated. Extravasated A555-cadaverine accumulates in neurons.[17] Scale bar 20 µm. **C**, Seventy kDa tetramethylrhodamine (TMR)-dextran accumulation into brains after 16-h circulation. **Lower** illustrates whole brains photographed after tracer circulation (*Mfsd2a*$^{+/+}$ n=4, *Mfsd2a*$^{-/-}$ n=5, and *Pdgfb*$^{ret/ret}$ n=3). **D**, Lipidomic analysis of aged *Pdgfb*$^{ret/ret}$ and *Pdgfb*$^{ret/ret}$ brains (*Pdgfb*$^{ret/+}$ n=7, *Pdgfb*$^{ret/ret}$ n=6). Data in **A** and **C** were normally distributed and significance was evaluated using 1-way ANOVA with Bonferroni multiple comparison test. Significance in **D** was evaluated using unpaired 2-tailed *t* test with Welch correction. Data are presented as geometric mean±geometric SD. DHA indicates docosahexaenoic acid; ns, not significant; PC, phosphatidylcholin; PE, phosphatidylethanolamine; and PS, phosphatidylserine.

(Figure 5C) following intravenous injection and circulation in adult awake *Mfsd2a*$^{-/-}$ or *Pdgfb*$^{ret/ret}$ mice. If MFSD2A mediates pericyte-suppressed EC transcytosis, we had expected to see similar or higher tracer leakage in *Mfsd2a*$^{-/-}$ than in *Pdgfb*$^{ret/ret}$ mice. However, under the experimental conditions used, neither tracer showed significantly increased accumulation in *Mfsd2a*$^{-/-}$ compared with *Mfsd2a*$^{+/+}$ brains, in marked contrast to the strong leakage observed in *Pdgfb*$^{ret/ret}$ brains (Figure 5A through 5C). MFSD2A has been shown to be a critical lipid transporter at the BBB, responsible for the transport of the essential omega-3 fatty acid docosahexaenoic acid into the brain,[47,65,66] and docosahexaenoic acid levels in *Mfsd2a*$^{-/-}$ brains are markedly reduced compared with controls.[47] In spite of the reduced MFSD2A levels observed in *Pdgfb*$^{ret/ret}$ brain vessels, lipidomic analysis did not reveal detectable changes in lipid composition in *Pdgfb*$^{ret/ret}$ brains (Figure 5D), suggesting that the residual MFSD2A expression observed in these mice is sufficient to maintain docosahexaenoic acid transport. Together, these observations demonstrate that the increased permeability of the *Pdgfb*$^{ret/ret}$ brain vasculature is caused by other mechanisms than loss of MFSD2A.

To address if the second candidate, FGFBP1, mediates or protects against the increased BBB permeability in *Pdgfb*$^{ret/ret}$ mice, we generated compound constitutive *Fgfbp1*$^{-/-}$;*Pdgfb*$^{ret/ret}$ mice and studied their vasculature in adult brains. Examining these mice for BBB permeability, we could not detect any increased leakage in single *Fgfbp1*$^{-/-}$ mice (*Pdgfb*$^{ret/+}$ background) nor could we detect increased leakage in double *Fgfbp1*$^{-/-}$:*Pdgfb*$^{ret/ret}$ versus single *Pdgfb*$^{ret/ret}$ mutants (Figure VIII in the Data Supplement). From these data, we conclude that FGFBP1 does not cause BBB leakage in *Pdgfb*$^{ret/ret}$ mice nor does it protect against it.

An Unexpected Role for *Angpt2* at the BBB

Although most of the strong sites of ANGPT2 expression observed in *Pdgfb*$^{ret/ret}$ mice did not colocalize with hotspot permeability sites (Figure 4B and 4C), *Angpt2*/ANGPT2 expression was generally increased in the EC of *Pdgfb*$^{ret/ret}$ brains (Figures 3A, 4B, and 4D and Figure VIID in the Data Supplement), particularly in EC devoid of pericyte contact (Figure 4D). To analyze if increased *Angpt2*/ANGPT2 expression contributes to the BBB defects observed in *Pdgfb*$^{ret/ret}$ mice, we induced deletion of *Angpt2* in *Pdgfb*$^{ret/ret}$ background. We generated *Pdgfb*$^{ret/ret}$:*Cdh5*-CreERT2:*Angpt2*$^{flox/flox}$ mice and induced deletion of *Angpt2* (*Pdgfb*$^{ret/ret}$;*Angpt2*^{ECKO}) by tamoxifen administration at 1 month of age, followed by analysis at 3 months of age. Contrary to our expectation, double *Pdgfb*$^{ret/ret}$;Angpt2^{iECKO} mutants were not protected against tracer leakage but instead showed a marked increase in the brain accumulation of 1 kDa A555-cadaverine in comparison with single *Pdgfb*$^{ret/ret}$ mice (Figure 6A). Immunofluorescent staining confirmed the efficient depletion of ANGPT2 in *Pdgfb*$^{ret/ret}$;*Angpt2*^{ECKO} mutants (Figure 6B).

The aggravated tracer leakage in the *Pdgfb*$^{ret/ret}$;*Angpt2*^{ECKO} mice was unexpected in view of the reported role for ANGPT2 in vessel destabilization. To further address this paradoxical result, we analyzed constitutive *Angpt2* knockout mice (*Angpt2*$^{-/-}$ mice), which demonstrated that also single *Angpt2*$^{-/-}$ mice displayed abnormal brain vascular morphology and increased leakage of A555-cadaverine tracer (Figure 6D). The mural cell abundance and zonation judged by pericyte and VSMC marker expression were normal in *Angpt2*$^{-/-}$ mice, pointing to a different mechanism(s) of BBB disruption than in *Pdgfb*$^{ret/ret}$ mice (Figure 6E). We, therefore, focused our attention to EC junction morphology and the expression of markers of adherens junctions (CDH5) and tight junctions (CLDN5). While the distribution of both proteins confirmed the expected abnormalities in EC shapes in the *Angpt2*$^{-/-}$ vessels, these displayed specific alterations in the distribution of CLDN5, which was both weaker and discontinuous along the cell-cell junctions, something that was not observed for CDH5 (Figure 6F). In contrast, control mice showed largely overlapping and continuous CDH5 and CLDN5 staining along the EC junctions. These data point to an important role for ANGPT2 in the development of CLDN5-containing tight junctions in the brain vasculature, as well as in maintenance of the integrity of these junctions during pericyte deficiency.

DISCUSSION

Our analysis provides detailed insight into how pericyte-deficiency changes the identity and behavior of brain EC in multiple ways with consequences for BBB integrity.

We found that the molecular A-V identity in EC was skewed in the pericyte-deficient brain. Out of 64 markers for brain venous EC, more than half were upregulated in *Pdgfb*$^{ret/ret}$ EC. Normally, a continuum of gene expression changes is observed along the A-V axis, including nested gene expression patterns of mRNAs coding for transcription factors, transporters, and other protein classes.[34] This A-V zonation is likely a prerequisite for proper positioning of vascular functions along the A-V axis, such as molecular transport and immune cell trafficking. The mechanisms establishing endothelial zonation in the brain and elsewhere are generally not known, but our current findings suggest a role for pericytes in this process.

We also addressed how pericyte deficiency affects organotypic specialization in the brain EC, that is, the molecular specification of the BBB phenotype. BBB function is impaired in the pericyte-deficient state,[3–5] but it has remained unclear how the pericyte-deficient BBB compares to other states of BBB-deficiency. Inhibition of Wnt signaling causes profound downregulation of BBB genes.[46] Our present results show that pericyte deficiency has comparably modest effects on the BBB. Most major BBB markers were normally expressed in *Pdgfb*$^{ret/ret}$ mice, and where differences were observed, they seemed to reflect a venous-shifted rather than dismantled BBB. The lipid transporter MFSD2A is an interesting exception, as its expression in brain ECs requires direct pericyte contact. However, the reduced MFSD2A expression observed in *Pdgfb*$^{ret/ret}$ mice was sufficed to maintain a normal brain lipid composition, and it did also not explain the BBB leakage, which was far more extensive in *Pdgfb*$^{ret/ret}$ mice than in *Mfsd2a*$^{-/-}$ under our experimental conditions.

The finding of angiogenic sprouts and typical tip cells was surprising considering the general vascular rarefaction in the adult *Pdgfb*$^{ret/ret}$ brain. Analysis of EC cycling, apoptosis, and total cell number suggested that the pericyte-deficient vessels were proliferatively quiescent. This provided us with an opportunity to molecularly characterize tip cells in absence of the concomitant vascular expansion that typically occurs during developmental and tumor angiogenesis. Indeed, we identified tip cells with a distinct gene and protein expression profile. While only a small number of tip cells was obtained, the depth of the SmartSeq2 technique provided meaningful information. To define markers unique for tip cells of the angiogenic sprout, we compared the tip (i-1) cells with the remaining cells (i-2) of the angiogenic cluster, which presumably include stalk cells. Of 112 enriched genes, 32 remained after multiple test correction. Clearly, this list is conservative. Moreover, because tip and stalk cells are known to dynamically switch position during angiogenic sprouting,[67] some lag in transcriptional changes between tip cells and stalk cells would be

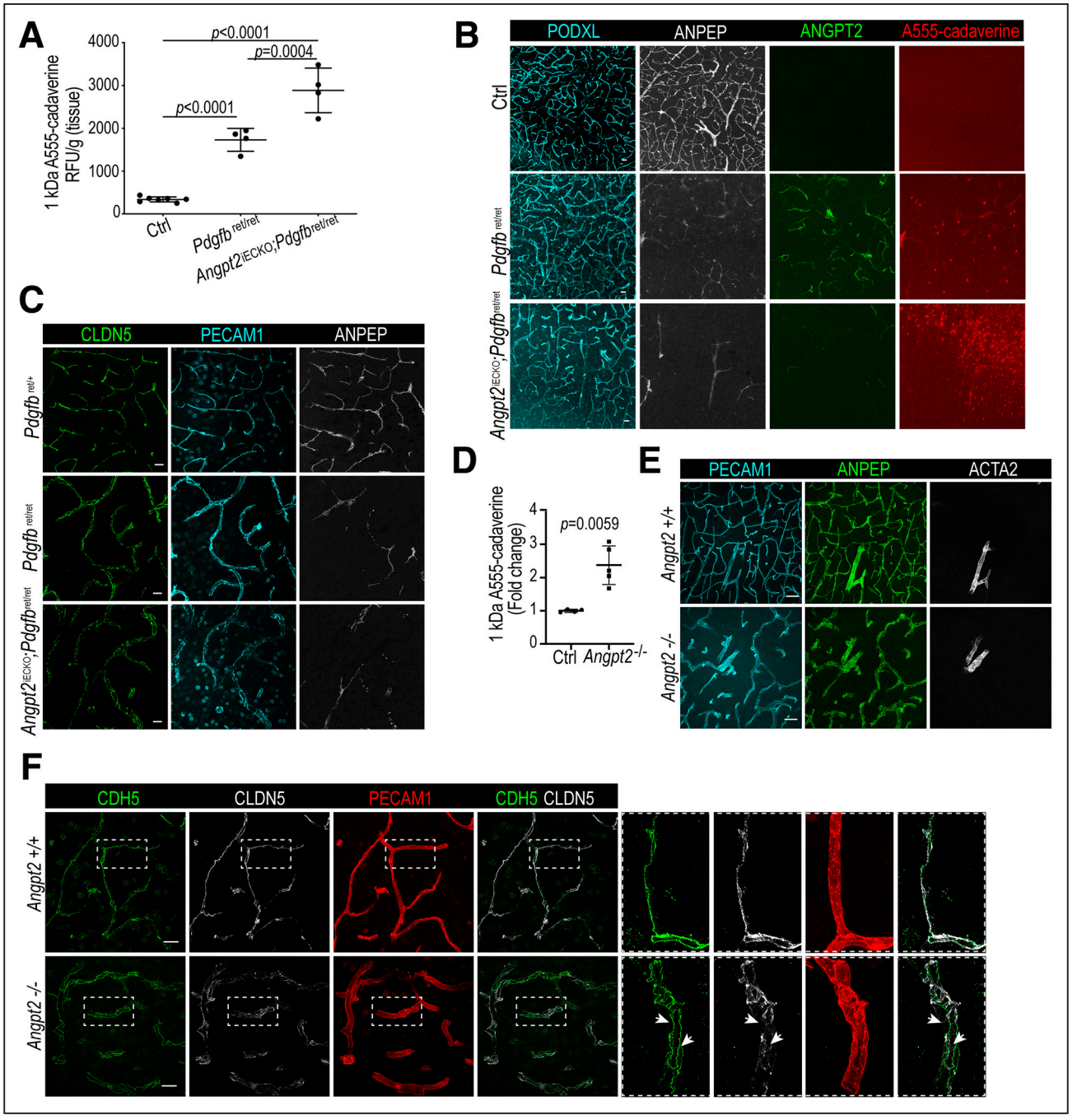

Figure 6. Role of Angpt2 (angiopoietin 2) at the blood-brain barrier (BBB).
A, Quantification of A555-cadaverine extravasation into brain tissue (Ctrl n=8, *Pdgfb*$^{ret/ret}$ n=4, *Angpt2*^{ECKO};*Pdgfb*$^{ret/ret}$ n=4, control genotypes provided in Methods). **B**, Three-dimensional reconstruction of confocal image z-stacks of cerebral neocortex vasculature depicted by immunofluorescent (IF) staining as indicated in *Ctrl*, *Pdgfb*$^{ret/ret}$ and *Angpt2*^{ECKO};*Pdgfb*$^{ret/ret}$ mice. Extravasated A555-cadaverine accumulates in neurons. Scale bar 20 μm. **C**, CLDN5 (Claudin 5) distribution is irregular in both *Pdgfb*$^{ret/ret}$ and *Angpt2*^{ECKO};*Pdgfb*$^{ret/ret}$ brains. Scale bar 20 μm. **D**, Quantification of the A555-cadaverine extravasation into brain tissue (Ctrl n=4, *Angpt2*$^{-/-}$ n=5, control genotypes are provided in Methods). **E**, Representative images of the vascular mural cell coverage in cerebral cortex (n=3). Scale bar 40 μm. **F**, Representative images of the CDH5 and CLDN5 junctional distribution in endothelial cell (EC) in cerebral cortex (n=3). Insets in *Angpt2*$^{+/+}$ illustrate continuous and overlapping CDH5 and CLDN5, whereas insets in *Angpt2*$^{-/-}$ show continuous CDH5 but discontinuous CLDN5 (arrows). Scale bar 20 μm. Data in **A** and **D** was normally distributed and significance evaluated using 1-way ANOVA with Bonferroni multiple comparison test. Data are presented as geometric mean±geometric SD.

expected, as also indicated by tSpace analysis, which positioned i-1 cells preferably at the distal part of the angiogenic branch. Nevertheless, the 32-gene list of tip cell- versus stalk cell-enriched transcripts includes *Mcam* and *Lamb1*, as well as previously proposed markers (*Cxcr4*,[56] *Pgf*,[59] *Kcna5*, *Sirpa*, and *Smoc2*[45])

along with several novels and unannotated transcripts, including micro-RNAs without known function. The erythropoietin receptor (*Epor*) mRNA was among the most distinct tip cell markers in our data set, which may be relevant in relation to the suggested roles for erythropoietin in tumor angiogenesis.[68] Intriguingly, many of the tip cell markers, including *Epor,* are shared with rare capillary-resident angiogenic precursors recently described in lymph nodes and other tissues.[42] The significance of this similarity remains to be investigated.

Previous analyses have established transcytosis as a major mode of tracer transport across the BBB in pericyte-deficient mice.[3,5] Our present analysis revealed extensive EC heterogeneity and a putative second mode of BBB impairment in *Pdgfb*$^{ret/ret}$ brains: hotspot leakage. By correlating mRNA profiles in the single-cell data with BBB permeability and protein expression patterns, we found that hotspot leakage sites had unique morphological and molecular characteristics, including the abnormal distribution of EC junctional molecules. Hotspot sites were hallmarked by low MFSD2A and low ANGPT2 expression. They also displayed high ICAM1 and detectable PLVAP, features of possible relevance for the observed focal extravasation of leukocytes.

The low ANGPT2 expression at the hotspot leakage sites in *Pdgfb*$^{ret/ret}$ brain was surprising as ANGPT2 is conceived mainly as a TIE2 receptor antagonist, promoting vascular destabilization and proinflammatory responses.[62,69–75] However, ANGPT2 has also been shown to exert context-dependent TIE2 agonistic activity, particularly in lymphatic endothelium or lymphatic-like vessels.[76–78] While we had anticipated that the upregulated expression of ANGPT2 in *Pdgfb*$^{ret/ret}$ mice exacerbated the BBB impairment, our data implicated the opposite because double *Pdgfb*$^{ret/ret}$;*Angpt2*^{ECKO} mice showed an aggravated rather than a rescued BBB function. That ANGPT2 exerts a protective rather than destabilizing function at the BBB was further supported by data from single *Angpt2*$^{-/-}$ mice, which showed increased tracer leakage, abnormal vascular morphology, and weak irregular junctional staining for CLDN5. If this reflects an agonistic role of ANGPT2 at the TIE2 receptor specifically in a BBB microenvironment remains to be investigated. TIE2 agonistic functions of ANGPT2 have been demonstrated in lymphatic EC, where they were linked to low expression of the TIE2 phosphatase VE-PTP (PTPRB).[77] However, our scRNA-seq data showed normal *Ptprb* expression in *Pdgfb*$^{ret/ret}$ EC (https://betsholtzlab.org/Publications/RetEC-scRNAseq/database.html).

Another proposed mechanism for ANGPT2-TIE2 agonistic function involves translocation of ANGPT2-TIE2-integrin complexes from the basement membrane to cell junctions, resulting in their stabilization and agonistic signaling.[79] Whether a specific molecular composition of the brain vascular basement membrane prevents binding to ANGPT2-TIE2-integrin complexes and instead promotes a junctional location with resulting stabilization and reinforcement of CLDN5-containing tight junctions remains an intriguing possibility for further study.

It is increasingly appreciated that primary vascular dysfunction may cause or accelerate neurological disease.[80,81] Conversely, neurodegenerative diseases may negatively affect brain vascular function.[82–84] Among the emerging links between neurodegenerative and cerebrovascular diseases, pericyte have received special attention.[85] Pericyte loss or dysfunction correlate with a wide range of neurological and neurodegenerative conditions, including diabetic retinopathy,[8] Alzheimer and other neurodegenerative diseases,[12–15,86–89] aging,[16] and stroke.[90] Mouse models of pericyte deficiency involving loss-of-function mutations in the *Pdgfb* or *Pdgfrb* genes or pericyte ablation by diphtheria toxin[91] display impaired BBB function,[3–5] reduced oxygen supply to the brain[91,92] and myelin degradation.[93] Hypomorphic *Pdgfb* mice also mimic primary familial brain calcification in humans[23,24] and display neurotoxic astrocyte activity and altered behavior and cognition suggestive of neuronal damage.[25] While all these studies point to a role for pericyte in overall brain function, it has remained unclear how pericyte deficiency affects their nearest neighbors, the ECs, at a molecular level. We undertook the present study using the most extensive, yet adult viable, mouse model of primary pericyte deficiency known, namely *Pdgfb*$^{ret/ret}$ mice,[3,19,20] in which ≈85% of the brain pericyte are lost, causing ≈75% of the capillary length to be devoid of visible pericyte contact. Because the *Pdgfb*$^{ret/ret}$ brain vasculature is sufficiently functional to support general brain functions and adult life, these mice are particularly suitable for analysis of how the EC phenotype changes when pericyte contact is missing. Our data show that the EC response to pericyte loss is complex, as may be expected also in aforementioned diseases. Our herein reported data and the appended online database https://betsholtzlab.org/Publications/RetECscRNAseq/database.html should guide further studies of pathogenic vascular states and their consequences in brain disease.

ARTICLE INFORMATION

Received May 19, 2020; revision received December 19, 2020; accepted December 28, 2020.

Affiliations

Department of Immunology, Genetics, and Pathology, Rudbeck Laboratory, Uppsala University, Sweden (M.A.M., L.H., S.N., E.V.-L., K.N., B.J., B.L., M.J., M.V., C.B.). Neurosurgery, Tianjin Medical University General Hospital, Tianjin Neurological Institute, Key Laboratory of Post-Neuroinjury Neuro-Repair and Regeneration in Central Nervous System, Ministry of Education and Tianjin City, China (L.H.). Pathology, Stanford University School of Medicine, CA (S.N., E.C.B.). Integrated Cardio Metabolic Center (ICMC) and Department of Medicine Huddinge, Karolinska Institutet Campus Flemingsberg, Sweden (X.L., M.J., M.V., C.B.). Duke-NUS Medical School, Singapore (B.C.T., D.L.S.). Singapore Lipidomics Incubator (SLING), Life Sciences Institute (J.C.F., A.C.-G., M.R.W.) and Biochemistry, Yong Loo Lin School of Medicine (A.C.-G., M.R.W.), National University of Singapore. Neurosurgery, Clinical Neuroscience Centrum, Zürich University Hospital, Zürich University

(Y.Z., A.K.). Medicine, Northwestern University, Feinberg School of Medicine, Chicago, IL (S.E.Q.). Neurobiology, Harvard Medical School, Boston, MA (C.G.).

Acknowledgments

This study was supported by the Swedish Research Council (C. Betsholtz: 2015-00550), the European Research Council (C. Betsholtz: AdG294556), the National Natural Science Foundation of China (L. He: 81870978), the Leducq Foundation (C. Betsholtz: 14CVD02), the Swedish Cancer Society (C. Betsholtz: 150735), Knut and Alice Wallenberg Foundation (C. Betsholtz: 2015.0030), Innovative Medicines Initiative (C. Betsholtz: IM2PACT-807015), the Swedish Society for Medical Research and Stanford Dean's Fellowship (S. Nordling) and NIH grants (E.C. Butcher: R01 AI130471 and CA228019). National Research Foundation grants, Singapore NRF2016NRF-NRFI001-15 and OF-IRG MOH-000217 (D.L. Silver). The computations were performed on resources provided by Swedish National Infrastructure for Computing through Uppsala Multidisciplinary Center for Advanced Computational Science (UPPMAX) under Project SNIC 2017/7-240 and sllstore2017069. We thank C. Olsson, H. Leksell, P. Peterson, and J. Chmielniakova for technical help. M.A. Mäe, A. Keller, and C. Betsholtz conceived and designed the project; M.A. Mäe, E. Vazquez-Liebanas, K. Nahar, M. Vanlandewijck, B. Jung, B.C. Tan, J.Chin Foo, A. Cazenave-Gassiot, M.R. Wenk, Y. Zarb, and B. Lavina performed experiments; L. He, S. Nordling, and X. Li performed bioinformatic analysis; L. He constructed the online database; S.E. Quaggin, M. Jeansson, and C. Gu provided essential reagents. M.A. Mäe, C. Betsholtz, L. He, S. Nordling, and E.C. Butcher analyzed the data; C. Betsholtz and M.A. Mäe wrote the article with substantial input from L. He, S. Nordling, E.C. Butcher, D.L. Silver, and A. Keller. All authors reviewed and approved the article.

Sources of Funding

None.

Disclosures

None.

Supplemental Materials

Detailed Methods
Online Figures I–VIII
Online Tables I–VI
References [94–98]

REFERENCES

1. Armulik A, Genové G, Betsholtz C. Pericytes: developmental, physiological, and pathological perspectives, problems, and promises. *Dev Cell.* 2011;21:193–215. doi: 10.1016/j.devcel.2011.07.001
2. Sims DE. The pericyte–a review. *Tissue Cell.* 1986;18:153–174. doi: 10.1016/0040-8166(86)90026-1
3. Armulik A, Genové G, Mäe M, Nisancioglu MH, Wallgard E, Niaudet C, He L, Norlin J, Lindblom P, Strittmatter K, et al. Pericytes regulate the blood-brain barrier. *Nature.* 2010;468:557–561. doi: 10.1038/nature09522
4. Bell RD, Winkler EA, Sagare AP, Singh I, LaRue B, Deane R, Zlokovic BV. Pericytes control key neurovascular functions and neuronal phenotype in the adult brain and during brain aging. *Neuron.* 2010;68:409–427. doi: 10.1016/j.neuron.2010.09.043
5. Daneman R, Zhou L, Kebede AA, Barres BA. Pericytes are required for blood-brain barrier integrity during embryogenesis. *Nature.* 2010;468:562–566. doi: 10.1038/nature09513
6. Park DY, Lee J, Kim J, Kim K, Hong S, Han S, Kubota Y, Augustin HG, Ding L, Kim JW, et al. Plastic roles of pericytes in the blood-retinal barrier. *Nat Commun.* 2017;8:15296. doi: 10.1038/ncomms15296
7. Török O, Schreiner B, Tsai HC, et al. Pericytes regulate vascular immune homeostasis in the CNS. *bioRxiv.* 2019:644120. doi: 10.1101/644120
8. Bresnick GH, Davis MD, Myers FL, de Venecia G. Clinicopathologic correlations in diabetic retinopathy. II. Clinical and histologic appearances of retinal capillary microaneurysms. *Arch Ophthalmol.* 1977;95:1215–1220. doi: 10.1001/archopht.1977.04450070113010
9. Enge M, Bjarnegård M, Gerhardt H, Gustafsson E, Kalén M, Asker N, Hammes HP, Shani M, Fässler R, Betsholtz C. Endothelium-specific platelet-derived growth factor-B ablation mimics diabetic retinopathy. *EMBO J.* 2002;21:4307–4316. doi: 10.1093/emboj/cdf418
10. Kusuhara S, Fukushima Y, Ogura S, Inoue N, Uemura A. Pathophysiology of diabetic retinopathy: the old and the new. *Diabetes Metab J.* 2018;42:364–376. doi: 10.4093/dmj.2018.0182
11. Fernández-Klett F, Priller J. Diverse functions of pericytes in cerebral blood flow regulation and ischemia. *J Cereb Blood Flow Metab.* 2015;35:883–887. doi: 10.1038/jcbfm.2015.60
12. Halliday MR, Rege SV, Ma Q, Zhao Z, Miller CA, Winkler EA, Zlokovic BV. Accelerated pericyte degeneration and blood-brain barrier breakdown in apolipoprotein E4 carriers with Alzheimer's disease. *J Cereb Blood Flow Metab.* 2016;36:216–227. doi: 10.1038/jcbfm.2015.44
13. Miners JS, Schulz I, Love S. Differing associations between Aβ accumulation, hypoperfusion, blood-brain barrier dysfunction and loss of PDGFRB pericyte marker in the precuneus and parietal white matter in Alzheimer's disease. *J Cereb Blood Flow Metab.* 2018;38:103–115. doi: 10.1177/0271678X17690761
14. Sengillo JD, Winkler EA, Walker CT, Sullivan JS, Johnson M, Zlokovic BV. Deficiency in mural vascular cells coincides with blood-brain barrier disruption in Alzheimer's disease. *Brain Pathol.* 2013;23:303–310. doi: 10.1111/bpa.12004
15. Winkler EA, Sengillo JD, Sullivan JS, Henkel JS, Appel SH, Zlokovic BV. Blood-spinal cord barrier breakdown and pericyte reductions in amyotrophic lateral sclerosis. *Acta Neuropathol.* 2013;125:111–120. doi: 10.1007/s00401-012-1039-8
16. Montagne A, Barnes SR, Sweeney MD, Halliday MR, Sagare AP, Zhao Z, Toga AW, Jacobs RE, Liu CY, Amezcua L, et al. Blood-brain barrier breakdown in the aging human hippocampus. *Neuron.* 2015;85:296–302. doi: 10.1016/j.neuron.2014.12.032
17. Lindahl P, Johansson BR, Levéen P, Betsholtz C. Pericyte loss and microaneurysm formation in PDGF-B-deficient mice. *Science.* 1997;277:242–245. doi: 10.1126/science.277.5323.242
18. Hellström M, Kalén M, Lindahl P, Abramsson A, Betsholtz C. Role of PDGF-B and PDGFR-beta in recruitment of vascular smooth muscle cells and pericytes during embryonic blood vessel formation in the mouse. *Development.* 1999;126:3047–3055.
19. Lindblom P, Gerhardt H, Liebner S, Abramsson A, Enge M, Hellstrom M, Backstrom G, Fredriksson S, Landegren U, Nystrom HC, et al. Endothelial PDGF-B retention is required for proper investment of pericytes in the microvessel wall. *Genes Dev.* 2003;17:1835–1840. doi: 10.1101/gad.266803
20. Abramsson A, Lindblom P, Betsholtz C. Endothelial and nonendothelial sources of PDGF-B regulate pericyte recruitment and influence vascular pattern formation in tumors. *J Clin Invest.* 2003;112:1142–1151. doi: 10.1172/JCI18549
21. Munk AS, Wang W, Bèchet NB, Eltanahy AM, Cheng AX, Sigurdsson B, Benraiss A, Mäe MA, Kress BT, Kelley DH, et al. PDGF-B is required for development of the glymphatic system. *Cell Rep.* 2019;26:2955–2969.e3. doi: 10.1016/j.celrep.2019.02.050
22. Zarb Y, Nassiri S, Utz SG, et al. Microglia control small vessel calcification via TREM2. *bioRxiv.* 2019:829341. doi: 10.1101/829341
23. Vanlandewijck M, Lebouvier T, Andaloussi Mäe M, Nahar K, Hornemann S, Kenkel D, Cunha SI, Lennartsson J, Boss A, Heldin CH, et al. Functional characterization of germline mutations in PDGFB and PDGFRB in primary familial brain calcification. *PLoS One.* 2015;10:e0143407. doi: 10.1371/journal.pone.0143407
24. Keller A, Westenberger A, Sobrido MJ, García-Murias M, Domingo A, Sears RL, Lemos RR, Ordoñez-Ugalde A, Nicolas G, da Cunha JE, et al. Mutations in the gene encoding PDGF-B cause brain calcifications in humans and mice. *Nat Genet.* 2013;45:1077–1082. doi: 10.1038/ng.2723
25. Zarb Y, Weber-Stadlbauer U, Kirschenbaum D, Kindler DR, Richetto J, Keller D, Rademakers R, Dickson DW, Pasch A, Byzova T, et al. Ossified blood vessels in primary familial brain calcification elicit a neurotoxic astrocyte response. *Brain.* 2019;142:885–902. doi: 10.1093/brain/awz032
26. Nahar K, Lebouvier T, Andaloussi Mäe M, Konzer A, Bergquist J, Zarb Y, Johansson B, Betsholtz C, Vanlandewijck M. Astrocyte-microglial association and matrix composition are common events in the natural history of primary familial brain calcification. *Brain Pathol.* 2020;30:446–464. doi: 10.1111/bpa.12787
27. Levéen P, Pekny M, Gebre-Medhin S, Swolin B, Larsson E, Betsholtz C. Mice deficient for PDGF B show renal, cardiovascular, and hematological abnormalities. *Genes Dev.* 1994;8:1875–1887. doi: 10.1101/gad.8.16.1875
28. Hellström M, Gerhardt H, Kalén M, Li X, Eriksson U, Wolburg H, Betsholtz C. Lack of pericytes leads to endothelial hyperplasia and abnormal vascular morphogenesis. *J Cell Biol.* 2001;153:543–553. doi: 10.1083/jcb.153.3.543
29. Gerhardt H, Golding M, Fruttiger M, Ruhrberg C, Lundkvist A, Abramsson A, Jeltsch M, Mitchell C, Alitalo K, Shima D, et al. VEGF guides angiogenic

sprouting utilizing endothelial tip cell filopodia. *J Cell Biol.* 2003;161:1163–1177. doi: 10.1083/jcb.200302047
30. He L, Vanlandewijck M, Raschperger E, et al. Analysis of the brain mural cell transcriptome. *Sci Rep.* 2016;6:35108. doi: 10.1038/srep35108
31. Jung B, Arnold TD, Raschperger E, Gaengel K, Betsholtz C. Visualization of vascular mural cells in developing brain using genetically labeled transgenic reporter mice. *J Cereb Blood Flow Metab.* 2018;38:456–468. doi: 10.1177/0271678X17697720
32. Grant RI, Hartmann DA, Underly RG, Berthiaume AA, Bhat NR, Shih AY. Organizational hierarchy and structural diversity of microvascular pericytes in adult mouse cortex. *J Cereb Blood Flow Metab.* 2019;39:411–425. doi: 10.1177/0271678X17732229
33. Picelli S, Faridani OR, Björklund AK, Winberg G, Sagasser S, Sandberg R. Full-length RNA-seq from single cells using Smart-seq2. *Nat Protoc.* 2014;9:171–181. doi: 10.1038/nprot.2014.006
34. Vanlandewijck M, He L, Mäe MA, Andrae J, Ando K, Del Gaudio F, Nahar K, Lebouvier T, Laviña B, Gouveia L, et al. A molecular atlas of cell types and zonation in the brain vasculature. *Nature.* 2018;554:475–480. doi: 10.1038/nature25739
35. Schaum N, Karkanias J, Neff N, et al. Single-cell transcriptomics of 20 mouse organs creates a Tabula Muris. *Nature.* 2018;562:367–372. doi: 10.1038/s41586-018-0590-4
36. Zeisel A, Hochgerner H, Lönnerberg P, Johnsson A, Memic F, van der Zwan J, Häring M, Braun E, Borm LE, La Manno G, et al. Molecular architecture of the mouse nervous system. *Cell.* 2018;174:999–1014.e22. doi: 10.1016/j.cell.2018.06.021
37. He L, Vanlandewijck M, Mäe MA, Andrae J, Ando K, Del Gaudio F, Nahar K, Lebouvier T, Laviña B, Gouveia L, et al. Single-cell RNA sequencing of mouse brain and lung vascular and vessel-associated cell types. *Sci Data.* 2018;5:180160. doi: 10.1038/sdata.2018.160
38. Fan J, Salathia N, Liu R, Kaeser GE, Yung YC, Herman JL, Kaper F, Fan JB, Zhang K, Chun J, et al. Characterizing transcriptional heterogeneity through pathway and gene set overdispersion analysis. *Nat Methods.* 2016;13:241–244. doi: 10.1038/nmeth.3734
39. van den Brink SC, Sage F, Vértesy Á, Spanjaard B, Peterson-Maduro J, Baron CS, Robin C, van Oudenaarden A. Single-cell sequencing reveals dissociation-induced gene expression in tissue subpopulations. *Nat Methods.* 2017;14:935–936. doi: 10.1038/nmeth.4437
40. Adam M, Potter AS, Potter SS. Psychrophilic proteases dramatically reduce single-cell RNA-seq artifacts: a molecular atlas of kidney development. *Development.* 2017;144:3625–3632. doi: 10.1242/dev.151142
41. Kalucka J, de Rooij LPMH, Goveia J, Rohlenova K, Dumas SJ, Meta E, Conchinha NV, Taverna F, Teuwen LA, Veys K, et al. Single-cell transcriptome atlas of murine endothelial cells. *Cell.* 2020;180:764–779.e20. doi: 10.1016/j.cell.2020.01.015
42. Brulois K, Rajaraman A, Szade A, Nordling S, Bogoslowski A, Dermadi D, Rahman M, Kiefel H, O'Hara E, Koning JJ, et al. A molecular map of murine lymph node blood vascular endothelium at single cell resolution. *Nat Commun.* 2020;11:3798. doi: 10.1038/s41467-020-17291-5
43. Dermadi D, Bscheider M, Bjegovic K, Lazarus NH, Szade A, Hadeiba H, Butcher EC. Exploration of cell development pathways through high-dimensional single cell analysis in trajectory space. *iScience.* 2020;23:100842. doi: 10.1016/j.isci.2020.100842
44. Xiang M, Grosso RA, Takeda A, Pan J, Bekkhus T, Brulois K, Dermadi D, Nordling S, Vanlandewijck M, Jalkanen S, et al. A single-cell transcriptional roadmap of the mouse and human lymph node lymphatic vasculature. *Front Cardiovasc Med.* 2020;7:52. doi: 10.3389/fcvm.2020.00052
45. Sabbagh MF, Heng JS, Luo C, Castanon RG, Nery JR, Rattner A, Goff LA, Ecker JR, Nathans J. Transcriptional and epigenomic landscapes of CNS and non-CNS vascular endothelial cells. *Elife.* 2018;7:e36187. doi: 10.7554/eLife.36187
46. Phoenix TN, Patmore DM, Boop S, Boulos N, Jacus MO, Patel YT, Roussel MF, Finkelstein D, Goumnerova L, Perreault S, et al. Medulloblastoma genotype dictates blood brain barrier phenotype. *Cancer Cell.* 2016;29:508–522. doi: 10.1016/j.ccell.2016.03.002
47. Nguyen LN, Ma D, Shui G, Wong P, Cazenave-Gassiot A, Zhang X, Wenk MR, Goh EL, Silver DL. Mfsd2a is a transporter for the essential omega-3 fatty acid docosahexaenoic acid. *Nature.* 2014;509:503–506. doi: 10.1038/nature13241
48. Kunz J, Krause D, Kremer M, Dermietzel R. The 140-kDa protein of blood-brain barrier-associated pericytes is identical to aminopeptidase N. *J Neurochem.* 1994;62:2375–2386. doi: 10.1046/j.1471-4159.1994.62062375.x
49. Madisen L, Zwingman TA, Sunkin SM, Oh SW, Zariwala HA, Gu H, Ng LL, Palmiter RD, Hawrylycz MJ, Jones AR, et al. A robust and high-throughput Cre reporting and characterization system for the whole mouse brain. *Nat Neurosci.* 2010;13:133–140. doi: 10.1038/nn.2467
50. Kurtz A, Wang HL, Darwiche N, Harris V, Wellstein A. Expression of a binding protein for FGF is associated with epithelial development and skin carcinogenesis. *Oncogene.* 1997;14:2671–2681. doi: 10.1038/sj.onc.1201117
51. Tassi E, Al-Attar A, Aigner A, Swift MR, McDonnell K, Karavanov A, Wellstein A. Enhancement of fibroblast growth factor (FGF) activity by an FGF-binding protein. *J Biol Chem.* 2001;276:40247–40253. doi: 10.1074/jbc.M104933200
52. Gibby KA, McDonnell K, Schmidt MO, Wellstein A. A distinct role for secreted fibroblast growth factor-binding proteins in development. *Proc Natl Acad Sci U S A.* 2009;106:8585–8590. doi: 10.1073/pnas.0810952106
53. Cottarelli A, Corada M, Beznoussenko GV, et al. Fgfbp1 promotes blood-brain barrier development by regulating collagen IV deposition and maintaining Wnt/beta-catenin signaling. *Development.* 2020;147:dev185140. doi: 10.1242/dev.185140
54. del Toro R, Prahst C, Mathivet T, Siegfried G, Kaminker JS, Larrivee B, Breant C, Duarte A, Takakura N, Fukamizu A, et al. Identification and functional analysis of endothelial tip cell-enriched genes. *Blood.* 2010;116:4025–4033. doi: 10.1182/blood-2010-02-270819
55. Heng JS, Rattner A, Stein-O'Brien GL, Winer BL, Jones BW, Vernon HJ, Goff LA, Nathans J. Hypoxia tolerance in the Norrin-deficient retina and the chronically hypoxic brain studied at single-cell resolution. *Proc Natl Acad Sci U S A.* 2019;116:9103–9114. doi: 10.1073/pnas.1821122116
56. Strasser GA, Kaminker JS, Tessier-Lavigne M. Microarray analysis of retinal endothelial tip cells identifies CXCR4 as a mediator of tip cell morphology and branching. *Blood.* 2010;115:5102–5110. doi: 10.1182/blood-2009-07-230284
57. Zhao Q, Eichten A, Parveen A, Adler C, Huang Y, Wang W, Ding Y, Adler A, Nevins T, Ni M, et al. Single-cell transcriptome analyses reveal endothelial cell heterogeneity in tumors and changes following antiangiogenic treatment. *Cancer Res.* 2018;78:2370–2382. doi: 10.1158/0008-5472.CAN-17-2728
58. Tsafrir D, Tsafrir I, Ein-Dor L, Zuk O, Notterman DA, Domany E. Sorting points into neighborhoods (SPIN): data analysis and visualization by ordering distance matrices. *Bioinformatics.* 2005;21:2301–2308. doi: 10.1093/bioinformatics/bti329
59. Goveia J, Rohlenova K, Taverna F, Treps L, Conradi LC, Pircher A, Geldhof V, de Rooij LPMH, Kalucka J, Sokol L, et al. An integrated gene expression landscape profiling approach to identify lung tumor endothelial cell heterogeneity and angiogenic candidates. *Cancer Cell.* 2020;37:421. doi: 10.1016/j.ccell.2020.03.002
60. Vanlandewijck M, Betsholtz C. Single-cell mRNA sequencing of the mouse brain vasculature. *Methods Mol Biol.* 2018;1846:309–324. doi: 10.1007/978-1-4939-8712-2_21
61. Haghverdi L, Lun ATL, Morgan MD, Marioni JC. Batch effects in single-cell RNA-sequencing data are corrected by matching mutual nearest neighbors. *Nat Biotechnol.* 2018;36:421–427. doi: 10.1038/nbt.4091
62. Augustin HG, Koh GY, Thurston G, Alitalo K. Control of vascular morphogenesis and homeostasis through the angiopoietin-Tie system. *Nat Rev Mol Cell Biol.* 2009;10:165–177. doi: 10.1038/nrm2639
63. Ben-Zvi A, Lacoste B, Kur E, Andreone BJ, Mayshar Y, Yan H, Gu C. Mfsd2a is critical for the formation and function of the blood-brain barrier. *Nature.* 2014;509:507–511. doi: 10.1038/nature13324
64. Andreone BJ, Chow BW, Tata A, Lacoste B, Ben-Zvi A, Bullock K, Deik AA, Ginty DD, Clish CB, Gu C. Blood-brain barrier permeability is regulated by lipid transport-dependent suppression of caveolae-mediated transcytosis. *Neuron.* 2017;94:581–594.e5. doi: 10.1016/j.neuron.2017.03.043
65. Alakbarzade V, Hameed A, Quek DQ, Chioza BA, Baple EL, Cazenave-Gassiot A, Nguyen LN, Wenk MR, Ahmad AQ, Sreekantan-Nair A, et al. A partially inactivating mutation in the sodium-dependent lysophosphatidylcholine transporter MFSD2A causes a non-lethal microcephaly syndrome. *Nat Genet.* 2015;47:814–817. doi: 10.1038/ng.3313
66. Guemez-Gamboa A, Nguyen LN, Yang H, Zaki MS, Kara M, Ben-Omran T, Akizu N, Rosti RO, Rosti B, Scott E, et al. Inactivating mutations in MFSD2A, required for omega-3 fatty acid transport in brain, cause a lethal microcephaly syndrome. *Nat Genet.* 2015;47:809–813. doi: 10.1038/ng.3311
67. Jakobsson L, Franco CA, Bentley K, Collins RT, Ponsioen B, Aspalter IM, Rosewell I, Busse M, Thurston G, Medvinsky A, et al. Endothelial cells dynamically compete for the tip cell position during angiogenic sprouting. *Nat Cell Biol.* 2010;12:943–953. doi: 10.1038/ncb2103

68. Annese T, Tamma R, Ruggieri S, Ribatti D. Erythropoietin in tumor angiogenesis. *Exp Cell Res.* 2019;374:266–273. doi: 10.1016/j.yexcr.2018.12.013
69. Benest AV, Kruse K, Savant S, Thomas M, Laib AM, Loos EK, Fiedler U, Augustin HG. Angiopoietin-2 is critical for cytokine-induced vascular leakage. *PLoS One.* 2013;8:e70459. doi: 10.1371/journal.pone.0070459
70. Fiedler U, Reiss Y, Scharpfenecker M, Grunow V, Koidl S, Thurston G, Gale NW, Witzenrath M, Rosseau S, Suttorp N, et al. Angiopoietin-2 sensitizes endothelial cells to TNF-alpha and has a crucial role in the induction of inflammation. *Nat Med.* 2006;12:235–239. doi: 10.1038/nm1351
71. Fiedler U, Scharpfenecker M, Koidl S, Hegen A, Grunow V, Schmidt JM, Kriz W, Thurston G, Augustin HG. The Tie-2 ligand angiopoietin-2 is stored in and rapidly released upon stimulation from endothelial cell Weibel-Palade bodies. *Blood.* 2004;103:4150–4156. doi: 10.1182/blood-2003-10-3685
72. Hu J, Srivastava K, Wieland M, Runge A, Mogler C, Besemfelder E, Terhardt D, Vogel MJ, Cao L, Korn C, et al. Endothelial cell-derived angiopoietin-2 controls liver regeneration as a spatiotemporal rheostat. *Science.* 2014;343:416–419. doi: 10.1126/science.1244880
73. Rathnakumar K, Savant S, Giri H, Ghosh A, Fisslthaler B, Fleming I, Ram U, Bera AK, Augustin HG, Dixit M. Angiopoietin-2 mediates thrombin-induced monocyte adhesion and endothelial permeability. *J Thromb Haemost.* 2016;14:1655–1667. doi: 10.1111/jth.13376
74. Scharpfenecker M, Fiedler U, Reiss Y, Augustin HG. The Tie-2 ligand angiopoietin-2 destabilizes quiescent endothelium through an internal autocrine loop mechanism. *J Cell Sci.* 2005;118:771–780. doi: 10.1242/jcs.01653
75. Ziegler T, Horstkotte J, Schwab C, Pfetsch V, Weinmann K, Dietzel S, Rohwedder I, Hinkel R, Gross L, Lee S, et al. Angiopoietin 2 mediates microvascular and hemodynamic alterations in sepsis. *J Clin Invest.* 2013;123:3436–3445. doi: 10.1172/JCI66549
76. Kenig-Kozlovsky Y, Scott RP, Onay T, Carota IA, Thomson BR, Gil HJ, Ramirez V, Yamaguchi S, Tanna CE, Heinen S, et al. Ascending vasa recta are angiopoietin/Tie2-dependent lymphatic-like vessels. *J Am Soc Nephrol.* 2018;29:1097–1107. doi: 10.1681/ASN.2017090962
77. Souma T, Thomson BR, Heinen S, Carota IA, Yamaguchi S, Onay T, Liu P, Ghosh AK, Li C, Eremina V, et al. Context-dependent functions of angiopoietin 2 are determined by the endothelial phosphatase VEPTP. *Proc Natl Acad Sci U S A.* 2018;115:1298–1303. doi: 10.1073/pnas.1714446115
78. Thomson BR, Heinen S, Jeansson M, Ghosh AK, Fatima A, Sung HK, Onay T, Chen H, Yamaguchi S, Economides AN, et al. A lymphatic defect causes ocular hypertension and glaucoma in mice. *J Clin Invest.* 2014;124:4320–4324. doi: 10.1172/JCI77162
79. Mirando AC, Shen J, Silva RLE, Chu Z, Sass NC, Lorenc VE, Green JJ, Campochiaro PA, Popel AS, Pandey NB. A collagen IV-derived peptide disrupts alpha5beta1 integrin and potentiates Ang2/Tie2 signaling. *JCI Insight.* 2019;4:e122043. doi:10.1172/jci.insight.122043
80. Iadecola C. The pathobiology of vascular dementia. *Neuron.* 2013;80:844–866. doi: 10.1016/j.neuron.2013.10.008
81. Zhao Z, Nelson AR, Betsholtz C, Zlokovic BV. Establishment and dysfunction of the blood-brain barrier. *Cell.* 2015;163:1064–1078. doi: 10.1016/j.cell.2015.10.067
82. Lendahl U, Nilsson P, Betsholtz C. Emerging links between cerebrovascular and neurodegenerative diseases-a special role for pericytes. *EMBO Rep.* 2019;20:e48070. doi: 10.15252/embr.201948070
83. Sweeney MD, Sagare AP, Zlokovic BV. Blood-brain barrier breakdown in Alzheimer disease and other neurodegenerative disorders. *Nat Rev Neurol.* 2018;14:133–150. doi: 10.1038/nrneurol.2017.188
84. Sweeney MD, Zhao Z, Montagne A, Nelson AR, Zlokovic BV. Blood-brain barrier: from physiology to disease and back. *Physiol Rev.* 2019;99:21–78. doi: 10.1152/physrev.00050.2017
85. Sweeney MD, Ayyadurai S, Zlokovic BV. Pericytes of the neurovascular unit: key functions and signaling pathways. *Nat Neurosci.* 2016;19:771–783. doi: 10.1038/nn.4288
86. Baloyannis SJ, Baloyannis IS. The vascular factor in Alzheimer's disease: a study in Golgi technique and electron microscopy. *J Neurol Sci.* 2012;322:117–121. doi: 10.1016/j.jns.2012.07.010
87. Farkas E, Luiten PG. Cerebral microvascular pathology in aging and Alzheimer's disease. *Prog Neurobiol.* 2001;64:575–611. doi: 10.1016/s0301-0082(00)00068-x
88. Nation DA, Sweeney MD, Montagne A, Sagare AP, D'Orazio LM, Pachicano M, Sepehrband F, Nelson AR, Buennagel DP, Harrington MG, et al. Blood-brain barrier breakdown is an early biomarker of human cognitive dysfunction. *Nat Med.* 2019;25:270–276. doi: 10.1038/s41591-018-0297-y
89. Sagare AP, Sweeney MD, Makshanoff J, Zlokovic BV. Shedding of soluble platelet-derived growth factor receptor-β from human brain pericytes. *Neurosci Lett.* 2015;607:97–101. doi: 10.1016/j.neulet.2015.09.025
90. Fernández-Klett F, Potas JR, Hilpert D, Blazej K, Radke J, Huck J, Engel O, Stenzel W, Genové G, Priller J. Early loss of pericytes and perivascular stromal cell-induced scar formation after stroke. *J Cereb Blood Flow Metab.* 2013;33:428–439. doi: 10.1038/jcbfm.2012.187
91. Nikolakopoulou AM, Montagne A, Kisler K, Dai Z, Wang Y, Huuskonen MT, Sagare AP, Lazic D, Sweeney MD, Kong P, et al. Pericyte loss leads to circulatory failure and pleiotrophin depletion causing neuron loss. *Nat Neurosci.* 2019;22:1089–1098. doi: 10.1038/s41593-019-0434-z
92. Kisler K, Nelson AR, Rege SV, Ramanathan A, Wang Y, Ahuja A, Lazic D, Tsai PS, Zhao Z, Zhou Y, et al. Pericyte degeneration leads to neurovascular uncoupling and limits oxygen supply to brain. *Nat Neurosci.* 2017;20:406–416. doi: 10.1038/nn.4489
93. Montagne A, Nikolakopoulou AM, Zhao Z, Sagare AP, Si G, Lazic D, Barnes SR, Daianu M, Ramanathan A, Go A, et al. Pericyte degeneration causes white matter dysfunction in the mouse central nervous system. *Nat Med.* 2018;24:326–337. doi: 10.1038/nm.4482
94. Kim D, Pertea G, Trapnell C, Pimentel H, Kelley R, Salzberg SL. TopHat2: accurate alignment of transcriptomes in the presence of insertions, deletions and gene fusions. *Genome Biol.* 2013;14:R36. doi: 10.1186/gb-2013-14-4-r36
95. Liao Y, Smyth GK, Shi W. featureCounts: an efficient general purpose program for assigning sequence reads to genomic features. *Bioinformatics.* 2014;30:923–930. doi: 10.1093/bioinformatics/btt656
96. Butler A, Hoffman P, Smibert P, Papalexi E, Satija R. Integrating single-cell transcriptomic data across different conditions, technologies, and species. *Nat Biotechnol.* 2018;36:411–420. doi: 10.1038/nbt.4096
97. van Dijk D, Sharma R, Nainys J, Yim K, Kathail P, Carr AJ, Burdziak C, Moon KR, Chaffer CL, Pattabiraman D, et al. Recovering gene interactions from single-cell data using data diffusion. *Cell.* 2018;174:716–729.e27. doi: 10.1016/j.cell.2018.05.061
98. Chan JP, Wong BH, Chin CF, Galam DLA, Foo JC, Wong LC, Ghosh S, Wenk MR, Cazenave-Gassiot A, Silver DL. The lysolipid transporter Mfsd2a regulates lipogenesis in the developing brain. *PLoS Biol.* 2018;16:e2006443. doi: 10.1371/journal.pbio.2006443